Nonlinear Dyn (2025) 113:17747–17768
https://doi.org/10.1007/s11071-025-11116-0

RESEARCH

Adaptive piezoelectric energy harvester using a shape memory alloy stopper

Arthur Adeodato · Lucas Lisboa Vignoli · Marcelo A. Savi · Luciana L. S. Monteiro

Received: 16 September 2024 / Accepted: 10 March 2025 / Published online: 2 April 2025

Abstract This paper investigates a novel adaptive energy harvester that synergistically combines piezoelectric material and shape memory alloy (SMA). The piezoelectric material converts mechanical into electrical energy while an SMA element is used as a stopper that introduces nonsmooth nonlinearity. Nonsmooth systems operate in different modes, with and without contact, presenting rich dynamics that can be useful to enhance energy harvesting capacity. Besides, the SMA can be exploited by considering two different behaviors: morphing ability to change the gap distance from temperature variations; energy dissipation due to hysteretic behavior during contact dynamical mode, contributing to the structural safety of the device. A mathematical model is proposed considering a linear constitutive model to describe the piezoelectric electromechanical behavior while a model with polynomial phase transformation kinetics is employed to describe SMA thermomechanical behavior. Numerical simulations are carried out evaluating the influence of nonlinear characteristics due to the contact and due to SMA phase transformations. The investigation establishes a comparison of the novel device with the linear device and with the nonlinear device with elastic stopper. Results show that the adaptive harvester has better performance for different operational conditions characterized by base amplitude and frequency. Therefore, the synergistic use of smart materials is a promising strategy to enhance energy harvesting capacity, especially considering ambient uncertainties.

A. Adeodato (✉)
Instituto Politécnico, Universidade do Estado do Rio de Janeiro, R. Bonfim, 25 - Vila Amélia, Nova Friburgo, RJ 28625-570, Brazil
e-mail: arthuradeodato@iprj.uerj.br

L. L. Vignoli
Center for Technology and Application of Composite Materials, Universidade Federal do Rio de Janeiro, Av. Aluízio da Silva Gomes, 50 - Bairro da Glória, Macaé, RJ 27930-560, Brazil
e-mail: ll.vignoli@mecanica.coppe.ufrj.br

M. A. Savi
Center for Nonlinear Mechanics, COPPE - Mechanical Engineering, Universidade Federal do Rio de Janeiro, Rio de Janeiro, RJ 21941-972, Brazil
e-mail: savi@mecanica.coppe.ufrj.br

L. L. S. Monteiro
Centro Federal de Educação Tecnológica Celso Suckow da Fonseca, CEFET/RJ - Department of Mechanical Engineering, Rio de Janeiro 20271-110, Brazil
e-mail: luciana.monteiro@cefet-rj.br

Keywords Energy harvesting · Piezoelectricity · Shape memory alloys · Nonsmooth systems · Discontinuous nonlinearities · Nonlinear dynamics

1 Introduction

The search for sustainable and efficient energy sources has been motivating the development of smart adaptive devices employed to power supply sensors and portable devices [36,44,66]. Smart materials emerged as an alternative to convert mechanical into electrical fields due to their multiphysical couplings [20,22]. Among several possibilities, piezoelectric materials are one of the most popular case employed in different applications related to oil drilling [64], aerospace structures [16,60], and biomedical devices [45].

Traditional piezoelectric energy harvesters are composed by a linear mechanical oscillator connected to an electrical circuit by a piezoelectric element [62]. On this basis, the maximum energy conversion condition is obtained when the external source frequency matches the system natural frequency and therefore, the harvester has good performance when operating under resonant conditions [6,21,55,61]. Since environmental energy sources present intrinsic uncertainties, the shift from the resonant condition promotes a critical decrease in the energy harvesting capacity [7]. Several design strategies have been developed to overcome these limitations [10].

In this regard, nonlinear energy harvesters are being explored to enhance harvesting capacity, establishing broadband devices [56]. Several strategies have been employed including mechanical, electrical and piezoelectric nonlinearities [59]. Chen et al. [12], Triplett et al. [57] discussed nonlinear electro-mechanical coupling of the piezoelectric transduction [13]. Mechanical nonlinearities are usually related to multistability, typically imposed by either magnetic interactions [14,26,53] or buckling [28,37].

Nonsmooth nonlinearity is another interesting alternative to increase system bandwidth. Discontinuous systems, associated with intermittent contacts between mechanical components, are employed for this aim [52]. Usually, these systems have complex nonlinear dynamics being identified in different mechanical systems such as drilling [5,18,43], rotordynamics [25], impact capsules and packages [32,33].

The mathematical modeling of nonsmooth systems involves equations of motion that operates in different modes, with and without contact, defining a switch model. Numerical procedures associated with these systems are challenging and usually require special treatments [17,47]. In general, unusual complex behaviors are expected for this kind of systems, including chaos, as can be observed in the following references: [11,39,41]. Experimental evidences assure the best approaches to treat nonsmooth systems. On this basis, Divenyi et al. [17] and Savi et al. [47] investigated a nonlinear oscillator with nonsmooth support. Different kinds of oscillators were treated by Liu et al. [34], Ma et al. [35], and Pavlovskaia et al. [42], showing the complex dynamics of nonsmooth systems.

The use of nonsmoothness in smart material systems can be useful for different purposes. Shape memory alloy (SMA) stoppers are an interesting approach to change the response complexity, avoiding undesirable dynamical situations. Basically, two kinds of phenomena can be exploited: the dissipation due to stress-induced hysteretic behavior; and the property change due to temperature-induced phase transformation. In this regard, dos Santos and Savi [19] investigated the nonlinear dynamics of a nonsmooth oscillator with an SMA stopper, showing the rich nonlinear response of the system and the use of the SMA phase transformations to attenuate critical vibration situations. The same idea was exploited in rotordynamical systems presenting similar qualitative behaviors by Silva et al. [50].

Nonsmoothness can be conveniently exploited to enhance the energy harvesting capacity. Nevertheless, it should be pointed out that, on one hand, the contact mode promotes a broader frequency range. On the other hand, there is a reduction of the response amplitude, which is associated with a decrease of the harvested power peak. Therefore, these characteristics needs to be properly designed in a dynamical perspective.

Blystad and Halvorsen [8] proposed an experimental apparatus to investigate the energy conversion phenomenon in a nonsmooth system with discontinuous linear stiffness support. Hardening effects were explored in order to obtain an increase of the system bandwidth. Later, Halim and Park [23] presented a theoretical–experimental analysis of low frequency contact systems. Zhou et al. [65] presented an investigation comparing uni and bilateral contacts. Essentially, the conclusions point to a competition between the bandwidth increase and the peak reductions to define the energy harvesting capacity. AI et al. [4] presented a parametric analysis considering a nonsmooth discontinuous piezoelectric energy harvester considering unilateral contacts.

Liu et al. [29], [30], [31] explored one and two-degrees of freedom harvesters with impacts while [24] evaluated a two-degree of freedom harvester with one piezoelectric element coupled to the first oscillator, comparing with one and two stoppers positioned close to the second oscillator. Alternative configurations for nonsmooth energy harvesters are being extensive investigated, being an innovative and challenging field [49].

The synergistic use of smart materials for energy harvesting purposes has been employed to enhance system capacity conferring adaptability characteristics to traditional harvesters. Adeodato et al. [1] and Arthur et al. [3] explored the adaptability of a piezoelectric energy harvester conferred by a shape memory alloy helical spring. The SMA thermomechanical behavior is employed, exploiting shape memory effect and mechanical property changes due to phase transformations. A proof-of-concept of the enhacement provied by synergistic use of smart materials is provided, showing numerical and experimental results using temperature-induced phase change provided by Joule's effect. The same idea was discussed by Silva et al. [51] that presented a parametric analysis evaluating the influence of temperature and mechanical loads. De Sousa et al. [15] provided experimental and numerical analyses of a typical aeroelastic section with shape memory alloy helical springs for energy harvesting from wind-structure interactions. Different values of SMA preload are evaluated aiming to control the resonance frequency together with the energy harvesting [63].

Specifically considering device configurations, Viet et al. [58] investigated a continuous composite beam made of two piezoelectric layers bounded to a pseudoelastic core for energy harvesting. The model was compared with 3D finite element simulations and results showed a consistent behavior compared with experimental data. Oudich and Thiebaud [38] explored the two-way shape memory effect in an SMA-piezoelectric double layer energy harvester. In this configuration, the SMA layer is allowed to associate one geometric shape for low temperatures and another for high temperatures while [48] treated a SMA-piezoelectric beam with tunable ability for energy harvesting, showing a shift around 10% on the natural frequency of the beam for the first three modes, allowing to tune the system to match with the external frequency. A general review comparing SMA and piezoelectric applications in composite material is presented by Thomas et al. [54].

Seeking for the advance of the synergistic use of smart material technologies and motivated by the enhancement of the energy harvesting capacity, this work investigates a novel adaptive piezoelectric energy harvester with an SMA adaptive stopper. The objective is to exploit the SMA morphing ability according to ambient changes, altering the gap by exploiting the shape memory effect induced by temperature variations. The nonsmooth nonlinearity is responsible for promoting dynamical changes. A linear model is employed to describe the piezoelectric effect while the SMA thermomechanical behavior is described by a constitutive model with assumed polynomial phase transformation kinetics [2]. On this basis, a mathematical model is proposed considering a nonsmooth thermo-electro-mechanical oscillator. Numerical simulations are of concern showing that the system adaptive behavior can properly alter system dynamics in order to enhance energy harvesting capacity. Two different aspects of the SMA support are exploited: morphing ability that changes the gap; hysteretic dissipation due to contact dynamical mode. Results show that the novel adaptive smart device presents better performance than the classical linear harvester or the one with elastic support.

After this introduction, the manuscript is organized into three sections. Section 2 deals with the mathematical modeling of the adaptive SMA-piezoelectric energy harvester. SMA constitutive model is treated and afterward, the equations of motion are formulated. Section 3 presents numerical simulations considering parametric analyses split into two parts: morphing the stopper position caused by temperature-induced phase transformations; stress-induced phase transformations due to contact where the pseudoelastic hysteretic behavior is exploited for vibration attenuation. Finally, Sect. 4 discusses final remarks.

2 Adaptive SMA-piezoelectric energy harvester

This section is dedicated to the mathematical modeling of a piezoelectric energy harvester with an adaptive SMA nonsmooth stopper. Initially, the SMA themomechanical behavior is described, presenting a constitutive model. Afterward, the conceptual model and the equations of motion are formulated for the energy harvester. Performance is accessed by the harvested power, also defined in this section.

2.1 SMA constitutive model

The SMA thermomechanical behavior is essentially related to the solid phase transformations that can be induced by either stress or temperature. Typically, there are two possible phases: austenite, stable in high temperatures and in a stress-free state; and martensite, stable at low temperatures and in a stress-free state. Martensitic phase has several variants that can be induced by stress field while austitic phase has only one variant.

The SMA macroscopic description can be represented by thermodynamical principles, being represented by consistent constitutive models. Some overviews of the most important models is presented by Lagoudas [27], Paiva and Savi [40], Savi [46]. By considering the stress σ, the strain ϵ and the temperature T, and assuming an internal variable that defines the volume fraction of martensite β, it is possible to present a general description of the SMA behavior. On this basis, the following constitutive equation is proposed based on the original work of Brinson [9], presented in the form of rates:

$$\dot{\sigma} = E\dot{\epsilon} + \alpha\dot{\beta} + \Xi\dot{T} \tag{1}$$

where the dots represent time derivative; $\alpha = -E\epsilon_R$ is the phase transformation parameter, where ϵ_R being the maximum recoverable strain coefficient; and Ξ is the thermal coefficient. E represents the Young's modulus that is defined from its value for the austenitic phase (E_A) and martensite (E_M), being expressed as a function of martensitic volume fraction (β): $E = E_A + \beta(E_M - E_A)$. On this basis, it should be noted that $\alpha = \alpha(\beta)$.

The two-way shape memory effect can be represented by a residual stress field that induces a martensitic variant. This residual stress is due to a training process necessary to promote the effect, that essentially, associates each phase to a specific shape, and the changes being induced by temperature variations, without mechanical loads.

On this basis, the constitutive equation can be written as difference equation, assuming initial condition represented with subscript 0 and a residual stress σ_r employed to respresent the two-way shape memory effect:

$$(\sigma - \sigma_0) + \sigma_r = E(\epsilon - \epsilon_0) + \alpha(\beta - \beta_0) + \Xi(T - T_0) \tag{2}$$

Phase transformation kinetics is described by an function, assumed to be a polynomial [2]. The phase transformation induced by temperature is described by the start and finish of critical temperatures: M_s and M_f for martensite; and A_s and A_f for austenite. On the other hand, critical stress phase transformation are defined by an surface represented by the following equations,

$$\begin{aligned} \sigma_{M_s} &= \sigma_s + C_M(T - M_s) \quad & \sigma_{A_s} &= C_A(T - A_s) \\ \sigma_{M_f} &= \sigma_f + C_M(T - M_f) \quad & \sigma_{A_f} &= C_A(T - A_f) \end{aligned} \tag{3}$$

where σ_{M_s} and σ_{M_f} represent the start and finish critical stresses for martensite while σ_{A_s} and σ_{A_f} represent the critical stresses for austenite formation; σ_s and σ_f are the start and finish values of stress for martensite reorientation due to mechanical load at low temperatures, while C_M and C_A are the slope of the curves in a stress temperature diagram according to Brinson [9].

The phase transformation kinetics is defined by a known function. The martensitic volume fraction is expressed as follows, respectively representing the austenite-martensite tranformation ($A \rightarrow M$) and martensite-austenite transformation ($M \rightarrow A$):

$$\beta = \beta_0 + (1 - \beta_0) f_M(\tilde{T}_M) \qquad A \rightarrow M \tag{4}$$

$$\beta = \beta_0 f_A(\tilde{T}_A) \qquad M \rightarrow A \tag{5}$$

where the normalized temperatures are defined as follows:

$$\tilde{T}_M = \frac{M_s - T}{M_s - M_f} \qquad A \rightarrow M \tag{6}$$

$$\tilde{T}_A = \frac{A_f - T}{A_f - A_s} \qquad M \rightarrow A \tag{7}$$

and the hardening functions $f_M(\tilde{T}_M)$ and $f_A(\tilde{T}_A)$ are expressed by two successive second order polynomial equations:

$$f_M(\tilde{T}_M) = \begin{cases} a_1\tilde{T}_M^2 & 0 \leqslant \tilde{T} \leqslant B_M \\ a_2\tilde{T}_M^2 + b_2\tilde{T}_M + c_2 & B_M < \tilde{T} \leqslant 1 \end{cases} \tag{8}$$

$$f_A(\tilde{T}_A) = \begin{cases} a_3\tilde{T}_A^2 + b_3\tilde{T}_A + c_3 & 1 \leqslant \tilde{T} \leqslant B_A \\ a_4\tilde{T}_A^2 & B_A < \tilde{T} \leqslant 0 \end{cases} \tag{9}$$

where $0 < B_M < 1$ and $0 < B_A < 1$ are parameters to define forward and reverse transformations, respectively, establishing start and finish of the polynomial curve. For forward phase transformation, the coefficients are set as: $a_1 = \frac{1}{B_M}$, $a_2 = \frac{1}{B_M-1}$, $b_2 = \frac{-2}{B_M-1}$, $c_2 = \frac{B_M}{B_M-1}$ while for reverse transformation, the values are: $a_3 = \frac{1}{B_A-1}$, $b_3 = \frac{-2}{B_A-1}$, $c_3 = \frac{B_A}{B_A-1}$, $a_4 = \frac{1}{B_A}$. These parameters can be used to adjust the phase transformation curve with experimental data for each specific SMA sample, being here adopted as $B_M = B_A = 0.5$ [2].

The two-way shape memory effect is represented by assuming a residual stress field $\sigma_r = E\epsilon_r$. Moreover, it is assumed that $\Xi = 0$.

2.2 Piezoelectric energy harvester

The proposed adaptive energy harvester conceptual design is composed by a piezoelastic cantilever beam with a tip mass in a capsule subjected to external stimulus that represents the ambient energy source, Fig. 1a. An SMA stopper confers a nonsmooth characteristic to the system, being characterized by a gap, g, that can change due to two-way shape memory effect. On this basis, a temperature variation induces the gap change. This mechanical system is coupled to an electric circuit by a piezolectric element.

Figure 1b presents the equivalent discrete model as a single degree of freedom oscillator characterized by the displacement $x = x(t)$ related to a inertial reference. Ambient energy source is represented by a base stimulus adopted to be harmonic $x_b = x_b(t) = X\sin(\omega t)$. The relative displacement is defined as $z = z(t) = x - x_b$. The overall mass of the system is considered to be concentrated at the inertial element represented by m. The restoring force of the beam is represented by the linear coefficient k_b associated with its stiffness. The dissipation effects involved in the device movement is represented by a linear viscous damping coefficient c_b while the piezoelectric coefficient is represented by θ. The SMA stopper is represented by a restitution force $F_s = \sigma S$, where $\sigma = \sigma(\epsilon, \beta, T)$ is described by the constitutive model discussed, and S being the SMA cross section. Besides, a linear viscous damping coefficient c_s represents other dissipations.

Figure 1c deals with the equivalent electrical circuit representation considering the piezoelectric element containing in internal electrical resistance (R_p), capacitance (C_p) and the electromecanical coupling as the product $\theta\dot{z}$. An external resistance (R_e) is connected in parallel with the piezoelectric element resulting in: $R_{eq} = (R_p \times R_e)/(R_p + R_e) \approx R_e$ assuming $R_e >> R_p$. $V = V(t)$ represents the electrical potential distance around the external resistance.

The system dynamics is characterized by two modes: without contact ($z < g$); and with contact ($z \geq g$). By applying the Newton's second law into the oscillator and the Kirchhoff's law for the electrical circuit, the governing equations for each dynamical mode can be written as follows:

$$\begin{aligned} &m\ddot{z} + c_b\dot{z} + k_b z - \theta V = -mA_b\sin(\omega t) \\ &\quad \text{if } z < g \text{ (without contact)} \\ &\theta\dot{z} + C_p\dot{V} + \frac{V}{R_e} = 0 \end{aligned} \tag{10}$$

$$\begin{aligned} &m\ddot{z} + (c_b + c_s)\dot{z} + k_b z + \sigma S - \theta V = -mA_b\sin(\omega t) \\ &\quad \text{if } z \geq g \text{ (with contact)} \\ &\theta\dot{z} + C_p\dot{V} + \frac{V}{R_e} = 0 \end{aligned} \tag{11}$$

where $A_b = -\omega^2 X$ is related to the base acceleration amplitude.

The SMA stopper employs the two-way shape memory effect to change the gap due to a temperature change. Therefore, the gap distance is defined as the difference between an initial gap, g_0, and the SMA recovered shape, being expressed according to the following equations:

$$g(g_0, T) = g_0 - \epsilon_R L_0[1 - \beta_0 f_A(\tilde{T})] \quad M \rightarrow A \tag{12}$$

$$g(g_0, T) = g_0 - \epsilon_R L_0[1 - (\beta_0 + (1 - \beta_0) f_m(\tilde{T}))] \quad A \rightarrow M \tag{13}$$

where L_0 is the initial SMA length. For low temperature condition, martensitic phase is stable, which means that $\beta = 1$ and the gap becomes g_0. For a high temperature condition, austenitic phase is stable and $\beta = 0$, leading to $g = \epsilon_R L_0$.

The harvester performance is defined in terms of the electrical variables of the external circuit. In this regard, the instantaneous electrical output power in the external resistance load can be expressed by:

$$P_{out} = \frac{1}{R_e}\int_{t_0}^{t} V^2 dt \tag{14}$$

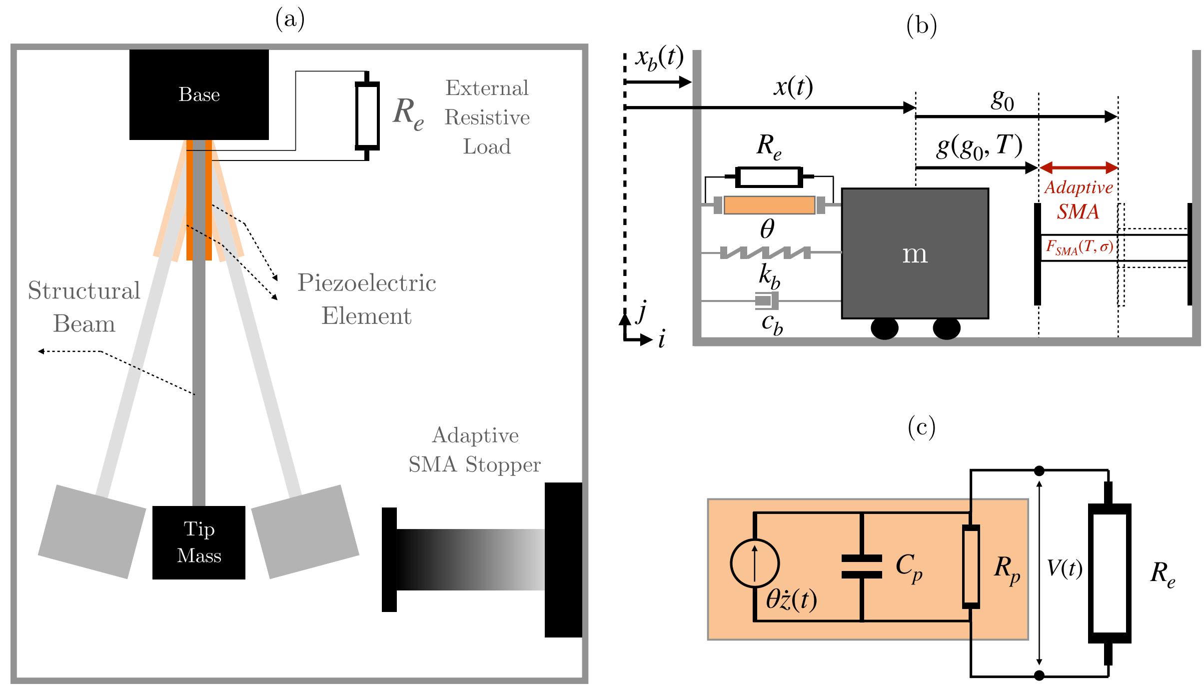

Fig. 1 System representation of the piezoelectric energy harvester with adaptive SMA stopper. **a** Physical model. **b** Lumped model of the harvester with discontinuous SMA stopper. **c** Equivalent electrical circuit with an external resistive load in parallel with the piezoelectric element

3 Results and discussion

This section deals with numerical simulations that employ the fourth-order Runge–Kutta method adopting time steps less than $dt = \tau \times 10^{-3}$, defined after a convergence analysis, where τ represents the forcing period. A total of 800 forcing periods is simulated considering that the harvester has achieved the steady state response after 80% of the total periods.

The investigation is split into two parts defined by the SMA stopper behavior: temperature-induced phase transformations; and stress-induced phase transformations. The first one deals with the adaptive characteristics of the harvester, associated with the SMA temperature control that alters the gap, promoting dynamical changes. The second part considers a constant temperature, associated with a specific gap, exploring pseudoelastic hysteretic dissipation due to stress-induced phase transformations that can attenuate critical vibration conditions.

The parameters for the oscillator are taken from Adeodato et al. [1] being presented in Table 1. The SMA stopper stiffness is assumed to be initially 10 times the system stiffness for ambient temperatures ($T < M_f$ where martensite phase is stable), while the dissipation is similar $c_s = c_b$, being consistent with AI et al. [4] dos Santos and Savi [19] and Savi et al. [47]. The properties of the shape memory alloy element considers the parameters presented in Table 2, being associated with a NiTi SMA commercial wire [2].

Initially, the SMA thermomechanical behavior is represented by considering a mechanical loading-unloading test at two distinct temperatures: high temperature $T = 291 > A_f$ - pseudoelasticity; and low temperature $T = 261 < M_f$ - shape memory effect. Figure 2 presents numerical simulations for the two cases, being represented by stress–strain-temperature curves, but also indicating the phases involved during the process. The high temperature behavior presents a elastic response followed by the phase transformation. An eleastic response occurs again in the sequel. The reverse behavior occurs during unloading, characterizing a hysteretic behavior. Note that, when the load is

Table 1 Parameters from the one degree of freedom piezoelectric energy harvester according to experimental procedures in Adeodato et al. [1]

m (kg)	k (N/m)	θ (N/V)	C_p (F)	$R_e(\Omega)$	c_b (N s/m)
0.01	213	-3.1×10^{-5}	2.48×10^{-8}	150×10^3	0.05

Table 2 SMA constitutive parameters according to experimental procedures in Adeodato et al. [2]

M_s (K)	M_f (K)	A_s (K)	A_f (K)	σ_s (MPa)	σ_f (MPa)
270.6	262.6	271.8	287.4	90.6	285.5
E_A (GPa)	E_M (GPa)	C_A (MPa/K)	C_M (MPa/K)	ϵ_R	$B_M = B_A$
43.2	18.9	7	6.5	0.06	0.5

removed, the SMA does not present any effect, but the process dissipates energy through the hysteresis. The low temperature behavior, on the other hand, presents a residual strain after unloading, which means that reverse phase transformation does not occur. Nevertheless, this residual strain can be eliminated by increasing the temperature, which promotes the temperature-induced phase transformation, recovering the initial shape.

The two-way shape memory effect is represented by a residual stress field, allowing the association of one shape for each temperature. This behavior allows one to change the gap distance of the SMA stopper based on the initial gap position (g_0) and the SMA temperature (T). Figure 3 shows an investigation of the gap distance relative to the initial gap g_0. Different curves are shown considering heating and cooling the SMA stopper for different values of stopper initial length (L_0). The start and finish SMA phase transformation temperatures are highlighted to show the region where phase transformation occurs. Note that, since the SMA residual strain coefficient is $\epsilon_R = 0.06$, the final gap becomes close to zero if the SMA initial length $L_0 = 16.66g_0$, according to Eq. (12). On the other hand, an SMA initial length $L_0 = 3.33g_0$ would present short capacity to promote a considerable change on the final gap distance. For this reason, an intermediate curve is chosen as $L_0 = 10g_0$ for further analyses and, as a consequence, the gap can vary in 60% of the initial gap. These observations compose one of the contributions of this paper that considers the SMA initial length with the ability to manipulate the gap distance in compact energy harvesters.

3.1 Temperature-induced phase transformations

A dynamical analysis of the energy harvester is now of concern considering situations related to temperature-induced phase transformations, which means that stress-induced phase transformations do not occur. This kind of behavior is associated with moderate external stimulus. A parametric analysis is developed allowing one to investigate the system performance over different conditions. Initially, a frequency response is investigated, promoting an up-sweep test varying the forcing frequency ω and evaluating the system maximum displacement. Different temperatures and, therefore, different gaps are analyzed. This allows one to build a 3D diagram showing frequency responses (displacement-frequency) for different temperatures (or gaps) (Fig. 4). The maximum displacement is presented in Fig. 4a while the maximum output power converted by the harvester is shown in Fig. 4b. By picking up a specific temperature to facilitate the visualization, a typical nonsmooth frequency response is observed and showed in Fig. 5. Note that the increase of frequency tends to increase the amplitude, but the nonsmooth nonlinearity deforms the classical resonant curve. This deformation is associated with a dynamical jump that occurs for a specific frequency. This behavior increases the frequency bandwidth of the system since a greater region of high amplitude response is observed.

These curves allow the analysis of different scenarios in terms of the gap distance as consequence of the SMA temperature variation and the shape memory effect. It should be pointed out that only temperature-induced phase transformations are occurring, which means that relative small base amplitudes are of con-

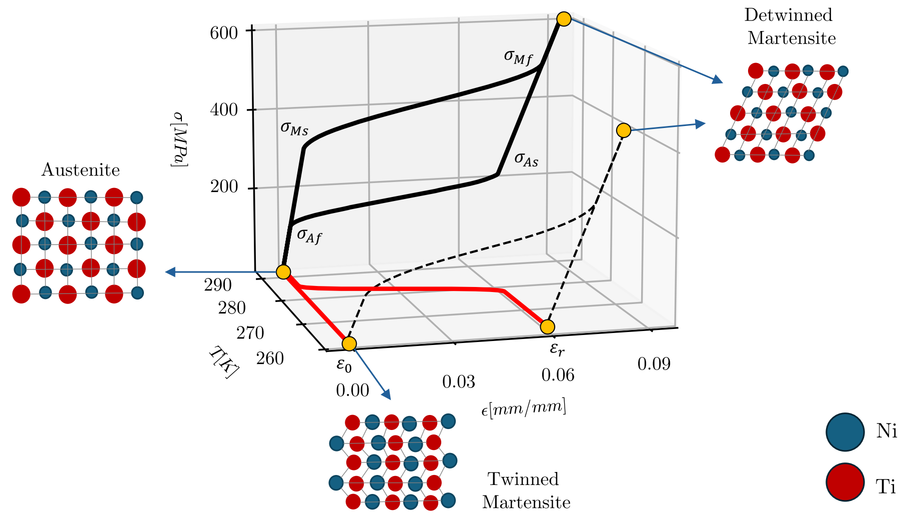

Fig. 2 SMA thermomechanical diagram concerning phase transformation induced by either stress and temperature fields. The phase transformation critical stresses are shown for pseudoelasticity at high temperatures while the residual strain ϵ_R remains for martensite reorientation processes at low temperarures

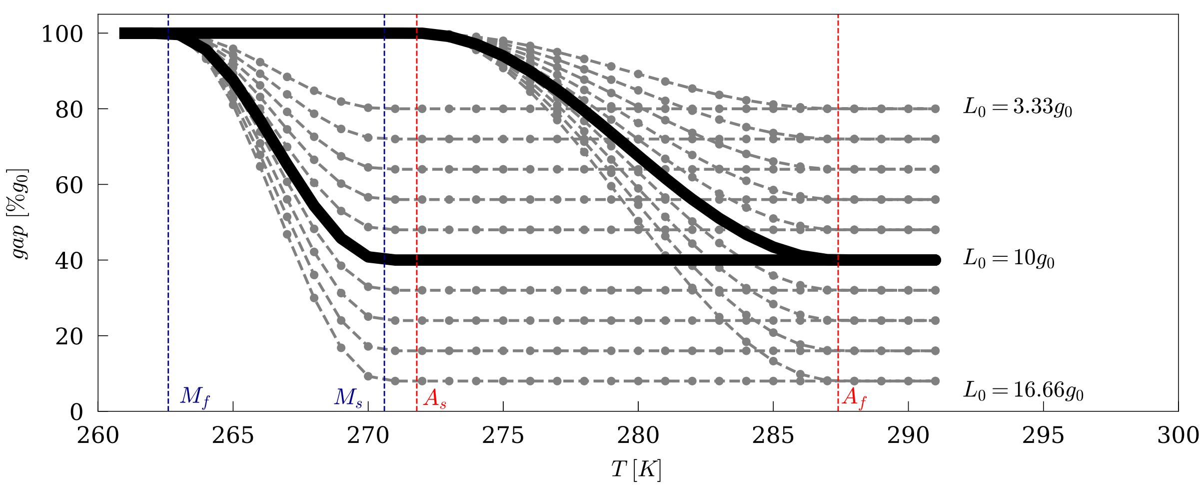

Fig. 3 The SMA stopper capacity to thermally control the final gap distance in terms of a percentage of the initial gap for different values of initial SMA length (L_0). Phase transformation critical temperatures are shown for martensite start M_s and final M_f, and austenite start A_s and final A_f according to Table 2

cern ($A_b = 1\,\text{m/s}^2$). This level of base amplitude is associated with the linear regime of the SMA stopper stress–strain relation. Nevertheless, different gap distances and stiffness associated with each temperature condition can be achieved. The maximum relative displacement and output power occur for $\omega = 146$ rad/s and their values are 1.37 mm and 4.47 µW, respectively. This happens when the SMA stopper temperature is less than M_f and therefore, the $g = g_0 = 1.5$ mm.

A different perspective of the system response is presented in Fig. 6 that shows color maps of Fig. 4 illustrating maximum displacement and output power converted for $A_b = 1$ m/s^2. Fig. 6a deals with the system maximum relative displacement and Fig. 6b presents the maximum output power by 2D colored surfaces associated with Fig. 4. Note that for low temperatures, where contact does not occurs, the system presents a linear response with the maximum power associated with the resonance condition followed by a considerable decay in performance under different conditions. Through Fig. 6b, it is possible to determine that for low temperatures, the system presents a range from 141 to 151 rad/s with consistent output power resulting in a interval of 10 rad/s where the system can operate

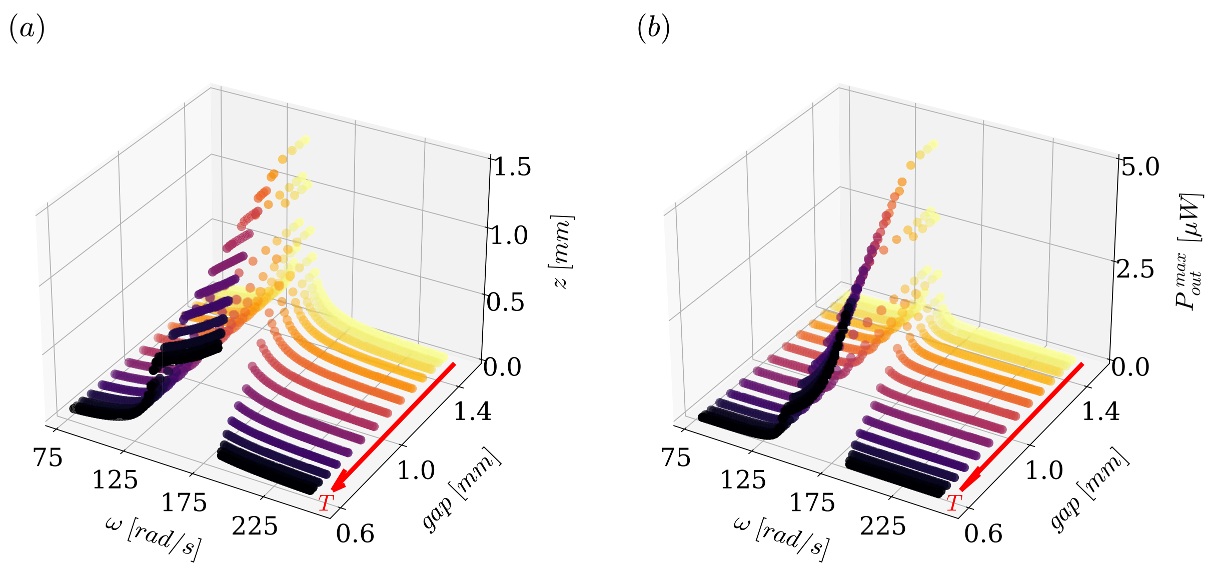

Fig. 4 Tridimensional diagram comparing the harvester performance in therms of forcing frequency ω and gap distance as a consequence of SMA shape memory effect. By increasing the SMA temperature T, the stopper expand and the gap becomes shorter. **a** Maximum relative displacement. **b** Maximum output power obtained

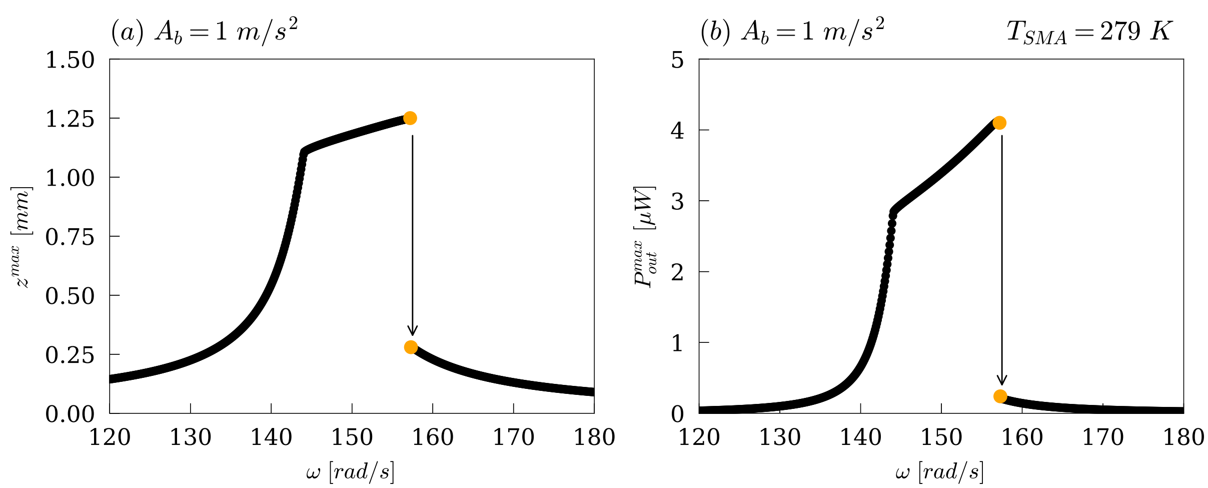

Fig. 5 Maximum response obtained in therms of forcing frequency ω for an specific SMA stopper temperature $T = 279$ K and low base vibration amplitude $A_b = 1\,\mathrm{ms}^2$. **a** Maximum relative displacement. **b** Output power

above 20% of the maximum power (0.89 μW). Alternatively, when the SMA temperature reaches A_s, phase transformation starts and the gap distance becomes smaller, increasing the system bandwidth in a nonlinear response. The system presents a range from 144.5 to 186.8 rad/s above 20% of the maximum output power, in a range of 42.3 rad/s. These results state that the frequency operational range can be extended more than 4 times.

Based on the value of the linear resonance frequency ($\omega_n = 146$ rad/s) when the stopper is at $T < M_f$ and the frequency associated with the maximum peak obtained from Fig. 6 when the stopper is at $T \geq A_f$ ($\omega_T = 186.6$ rad/s), it is possible to find the temperature that the stopper must be for a given excitation frequency between this range considering a linear relation between both conditions of resonance and connected by the martensitic volume fraction. On this basis, concerning a nonlinear governing law for β, an interpolation between the peak points may be developed and one derives the following expression to represent the envelope of the output power boundary in Fig. 6: $\omega = \omega_T + \beta(\tilde{T})(\omega_n - \omega_T)$. Hence:

$$\beta(\tilde{T}) = \frac{\omega - \omega_T}{\omega_n - \omega_T} = \begin{cases} a_3\tilde{T}_A^2 + b_3\tilde{T}_A + c_3 & 1 \leqslant \tilde{T} \leqslant B_A \\ a_4\tilde{T}_A^2 & B_A < \tilde{T} \leqslant 0 \end{cases} \tag{15}$$

and T can be determined by solving Eq. (15) and according to $T = A_f - \tilde{T}(A_f - A_s)$.
If $1 \leqslant \tilde{T} \leqslant B_A$

$$\left[\frac{a_3}{(A_f - A_s)^2}\right]T^2 - \left[A_f\left(\frac{2a_3}{(A_f - A_s)^2} + \frac{b_3}{(A_f - A_s)}\right)\right] T = \left(\frac{\omega - \omega_T}{\omega_n - \omega_T}\right) - \left(c_3 + \frac{a_3 A_f^2}{(A_f - A_s)^2} + \frac{b_3}{(A_f - A_s)}\right) \tag{16}$$

If $B_A < \tilde{T} \leqslant 0$

$$T = A_f - (A_f - A_s)\sqrt{\frac{\omega - \omega_T}{a_4(\omega_n - \omega_T)}} \tag{17}$$

The curves referred to Eqs. (16) and (17) are shown in Fig. 6a where it is possible to observe a critical difference. This is associated with the fact that even when SMA phase transformation starts, and the gap becomes smaller, the contact still not occurring until the gap assumes the value of the maximum linear displacement. The adjust of the curve can be done by substituting the variable A_s at Eqs. (16) and (17) by A_s', the temperature where the contact starts to occur. This difference is showed in Fig. 6a allowing one to determine the temperature where the stopper needs to be for a given external forcing frequency. These set of equations from Eq. (15) to Eq. (17) provides a novel procedure to tune the harvester dynamical response through the SMA thermomechanical coupling during low energy contact conditions that is going to be explored next.

Based on that, a dynamical investigation is now in focus showing situations where the variation of the forcing frequency can be compensated by the change of the SMA temperature, adjusting the harverter to keep a good performance. Three conditions of SMA temperatures are selected for a detailed analysis, presented in Fig. 7. On this basis, consider an operational condition at $\omega = 146$ rad/s. For a low temperature condition ($T < M_f$) related to the SMA stopper at full martensitic phase, the gap is $g = g_0 = 1.5$ and dynamics is in noncontact mode, presenting a good perfomance. The increase of the forcing frequency changes the harvesting capacity, and a thermal load can be applied in the SMA stopper until $T = 279$ K, changing the gap to $g = 1.1$ mm. This movement is represented by yellow dots in Fig. 7. In this regard, it is noticeable a nonlinear response attributed to the contact where the system operational range suffers an increase until 157 rad/s, followed by a dynamical jump from 4.12 to 0.2 μW. This effect can be even more prominent for $T = 291$ K where the SMA presents full austenitic phase and $g = 0.6$ mm, which means that the harvester can keep working until 186.8 rad/s with 3.7 μW. Two nonlinear phenomena are involved in this situation. The first is the nonsmoothness related to the contact, promoted by the SMA temperature; the second is the stopper stiffness, associated with the SMA elastic modulus of each phase, varying from E_M to E_A, which changes bandwidth.

The adaptive characteristic is now investigated through time domain analyses following the path described by the yellow dots in Fig. 7. Figure 8 presents results considering 200 forcing periods for each interval of frequency, which ensures that the steady state response is reached. Figure 8a presents time series for relative displacement and Fig. 8b for output power in a situation where the forcing frequency starts at $\omega = 146$ and low temperature $T = 271$ K, without contact, and therefore, with a linear response. The system performance is enhanced by heating the SMA stopper to $T = 279$ K, leading the system to a nonlinear response due to contact. The SMA stopper now presents both martensitic and austenitic phases and the stopper stiffness is increased compared to the previous condition. Afterward, the forcing frequency starts to increase from 146 to 150 and 155 rad/s when it is possible to note an increase of the total output power, as showed in Fig. 8b. A comparative analysis is shown in gray curves that SMA stopper is not activated, clearly establishing the difference in the system response. By continuing to increase the forcing frequency to $\omega = 170$ and 180 rad/s, the system may be heated to $T = 291$ K where the

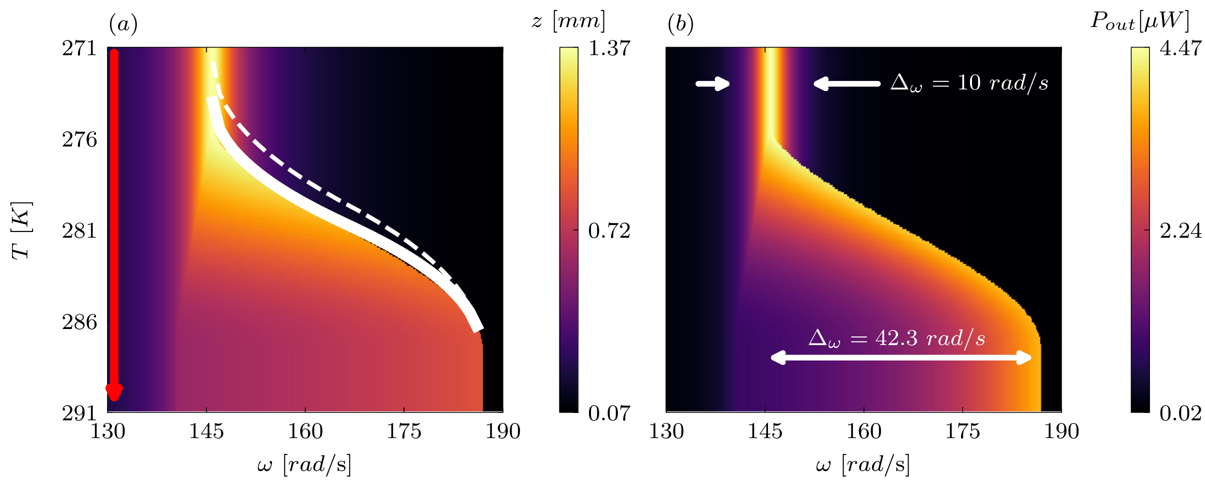

Fig. 6 Maximum distribution surface in therms of forcing frequency ω and SMA stopper temperature (T). **a** Maximum relative displacement **b** Output power

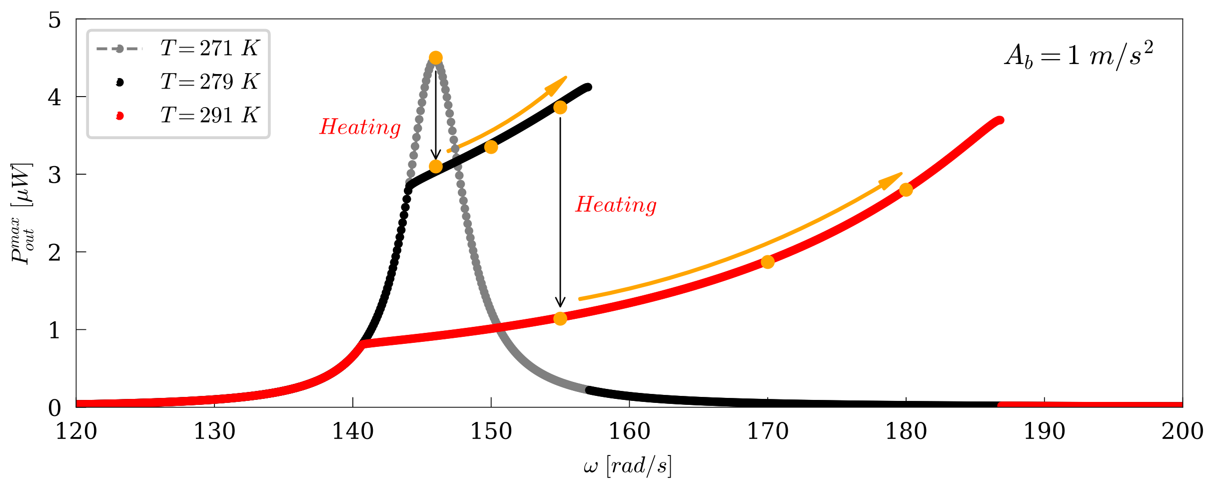

Fig. 7 Adaptive output power frequency response for different conditions of SMA stopper temperature (T) associated to gap distances. A representative path following optimal conditions is indicated for base amplitude $A_b = 1$ m/s^2

relative displacement is considerably bigger than the situation where the SMA temperature does not change.

The performance metrics considers the mean of the output power for the total curve presented in Fig. 8b. The linear case, without SMA actuation, presents 0.7 μW as the total mean while the adaptive stopper presents 1.44 μW. The difference represents twice the mean output power for the SMA adaptive stopper when compared with a linear harvester over the 30 s.

The harvester dynamics is now investigated in Fig. 9 with results for steady state response at selected stationary forcing frequencies: 146, 155, and 186 rad/s. Different conditions can be achieved by controlling the SMA temperature and the gap distance according to the phase spaces in Fig. 9c, f, and i, respectively. For $\omega =$ 146 rad/s, the linear response, plotted in gray lines, presents the good performance condition with larger displacement and output power, followed by the condition associated with $T = 271$ K and $T = 291$ K. For $\omega = 155$ rad/s, contact occurs when the SMA is activated and the best performance is now associated with $T = 279$ K, followed by $T = 291$ K. Note that under these conditions, the contact still occurring in the steady state response which promotes a better perfor-

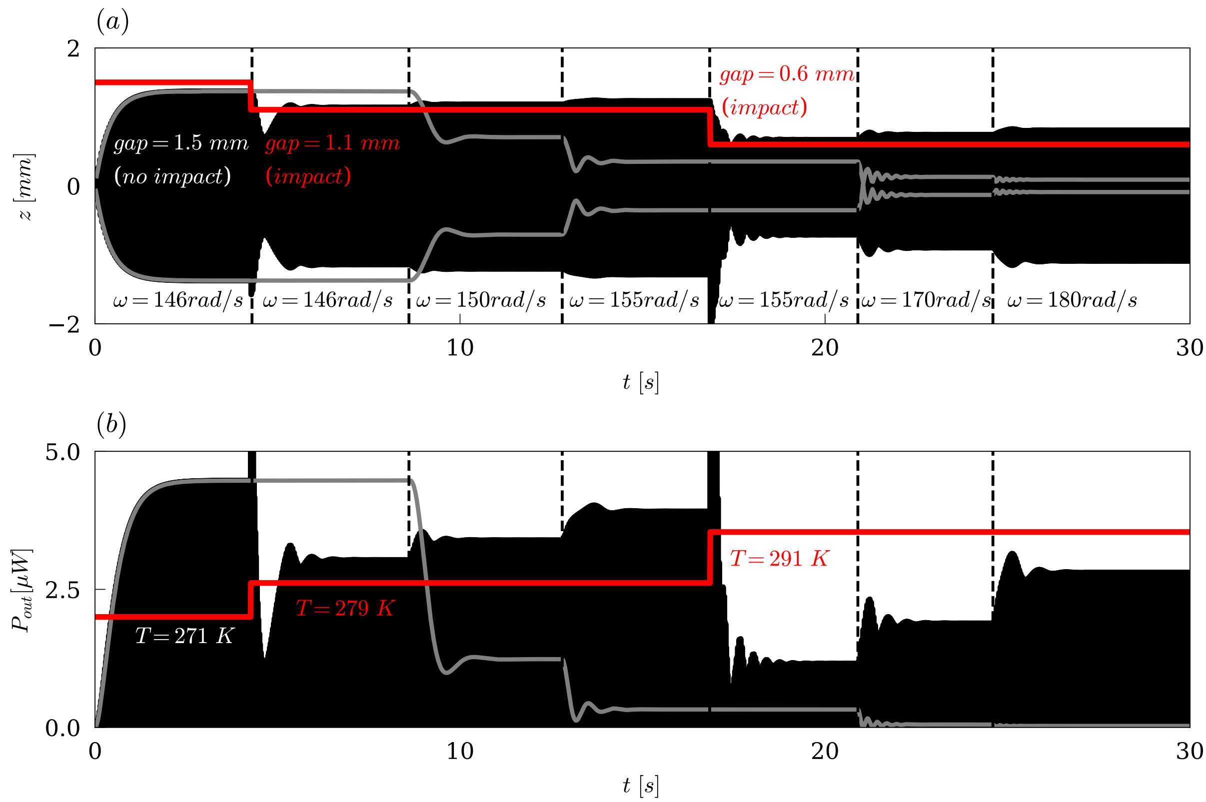

Fig. 8 Adaptptive harvester response for increasing forcing frequency ω and SMA temperature (T) change from 271 K to 291 K. **a** Relative displacement. **b** Output power

mance than the linear case for $T = 271$ K. Finally, for $\omega = 180$ rad/s, the best condition is related to $T = 291$ K, where the phase space is considerably affected by the contact with the SMA stopper. With $T = 271$ K and 279 K no contact occurs and both conditions are associated with a linear response.

3.2 Stress-induced phase transformations

The previous section discussed the adaptive behavior of the energy harvester considering low energy level situations, where amplitudes are not enough to promote stress-induced phase transformations. This section deals with situations where these phase transformations can be induced. On this basis, the peseudoelastic effect is of concern and hysteretic behavior is the main phenomenon behind the system response. This behavior dissipates energy, being expected to reduce energy harvesting capacity, but also contributing to the device safety and durability. Therefore, the objective of the present investigation is to explore the pseudoelastic effect on the SMA stopper due to the contact for higher base vibration amplitudes (A_b). It is assumed a constant temperature $T = 291$ K and gap distance $g_0 = 0.6$ mm. The SMA stopper now starts in fully austenitic phase and numerical simulations are performed with time steps $dt = (1/3)\tau \times 10^{-3}$, smaller than the previous cases.

Fig. 10a presents results for maximum relative displacements in up-sweep frequency analysis while Fig. 10b deals with the maximum martensitic volume fraction for different values of A_b. The pseudoelastic effect confers an additional nonlinearity that shifts the maximum peak frequency depending on the base amplitude. Complex nonlinear dynamics are detected, specifically multiple dynamical jumps and multi-periodic orbits. The total amount of martensitic phase, represented by the volume fraction β formed during the contact, can be associated with the dissi-

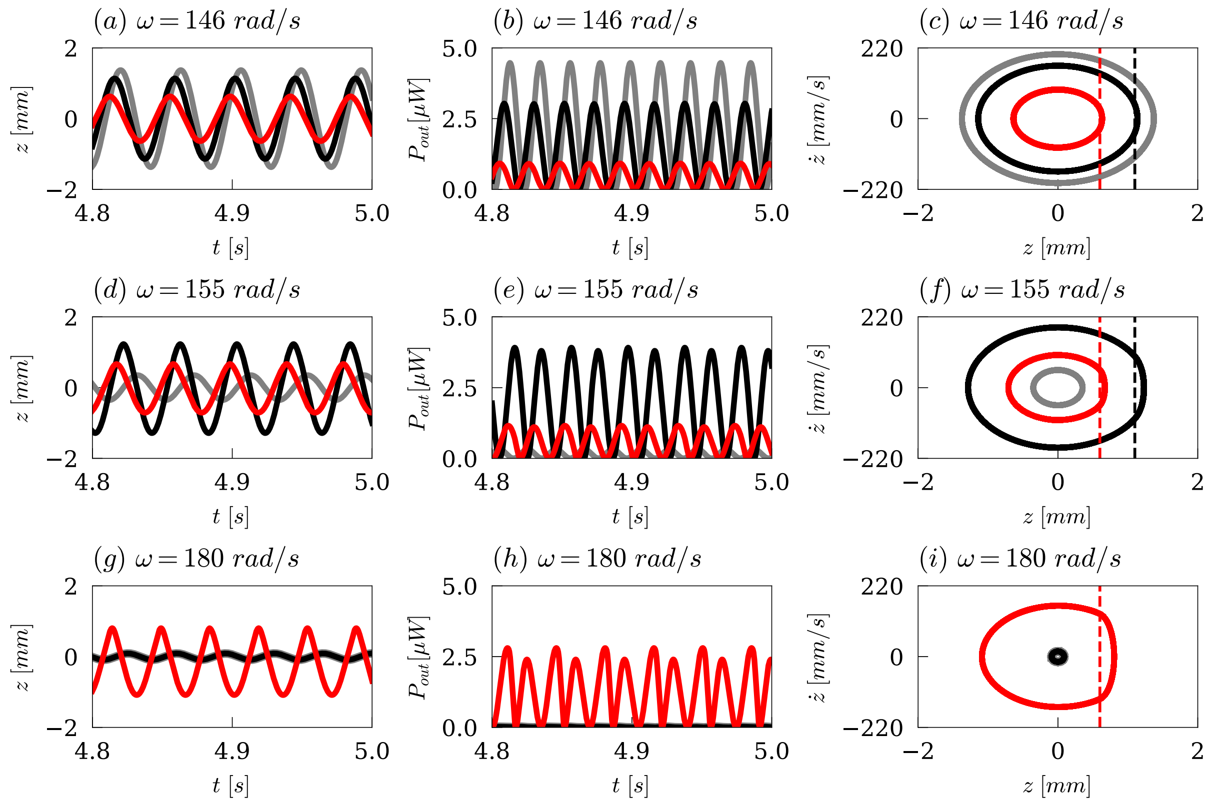

Fig. 9 Steady state response for the adaptive SMA piezoelectric harvester for stationary forcing frequency. **a**–**c** for $\omega = 146$ rad/s. **d**–**f** for $\omega = 155$ rad/s. **g**–**f** for $\omega = 180$ rad/s

pated energy allowing the harvester to support severe conditions of vibration amplitudes.

Fig. 11 shows a bidimensional colored surface associated with Fig. 10. When phase transformation occurs, three phenomena are related to the nonlinear response: nonsmoothness; stiffness variation; hysteretic energy dissipation. The relative displacement (Fig. 11a) can be smoothed through the softening effect associated with martensitic transformation. The region of high energy motion is extended from a single peak (linear response) to multiples peaks according to the level of base amplitude. Figure 11b deals with the martensitic volume fraction formed during the contacts.

In the sequel, results present the harvester output power frequency response highlighting interesting conditions for steady state analysis. Figure 12a presents the output frequency response associated with the analyses in Figs. 10 and 11, highlighting the region from 121 to 128 rad/s where the system response shifts from period-1 to a period-3 response for $A_b = 4\,\mathrm{m/s^2}$. Note that for this interval, the maximum output power response becomes closer to the harvester response for $A_b = 6$ and $8\,\mathrm{m/s^2}$.

As an example, a stationary frequency of $\omega = 125$ rad/s is selected and its steady state response is presented in Fig. 12b–d, showing the relative displacement, the output power times series and the phase space with the referred Poincaré sections, respectively. Under this condition, stress-induced phase transformation does not occur. Therefore, the transition to a period-3 orbit is associated with the nonsmooth nonlinearity. In addition, the maximum output power for $A_b = 4\,\mathrm{m/2^2}$ occurs at $\omega = 169$ rad/s with 7.8 μW followed by a dynamical jump between 180 and 181 rad/s. The dynamical jump is now associated with two phenomena as the contact and the transition from a condition where incomplete SMA phase transformation occurs, to a condition where phase transformation does not occur any more.

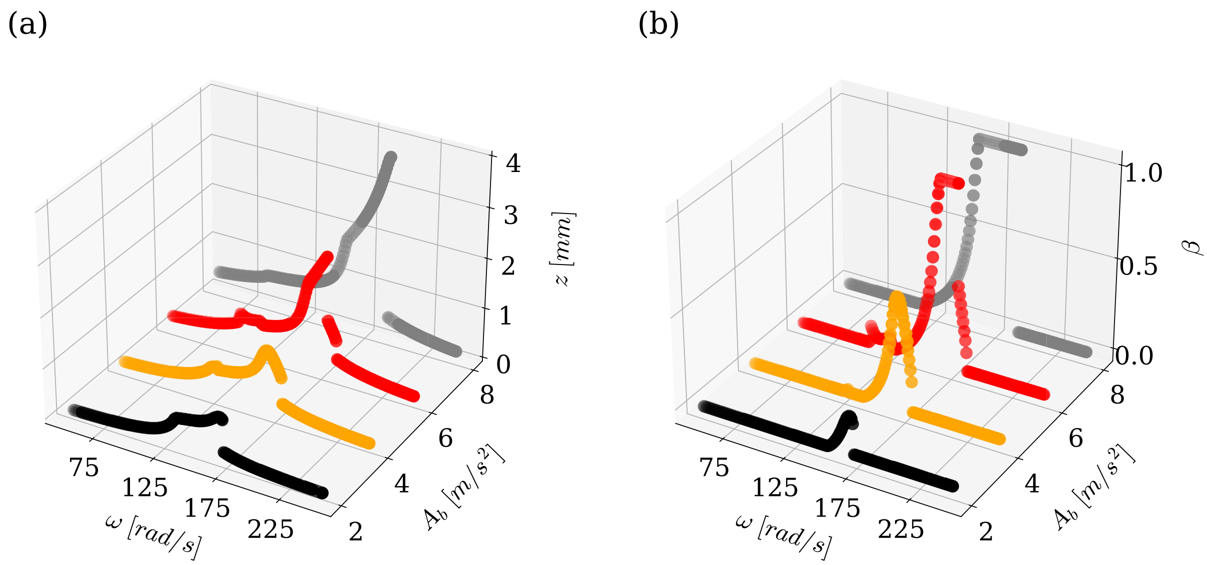

Fig. 10 Tridimensional diagram comparing the harvester performance in therms of forcing frequency ω and forcing amplitude A_b. **a** Maximum relative displacement. **b** Maximum Martensite volume fraction

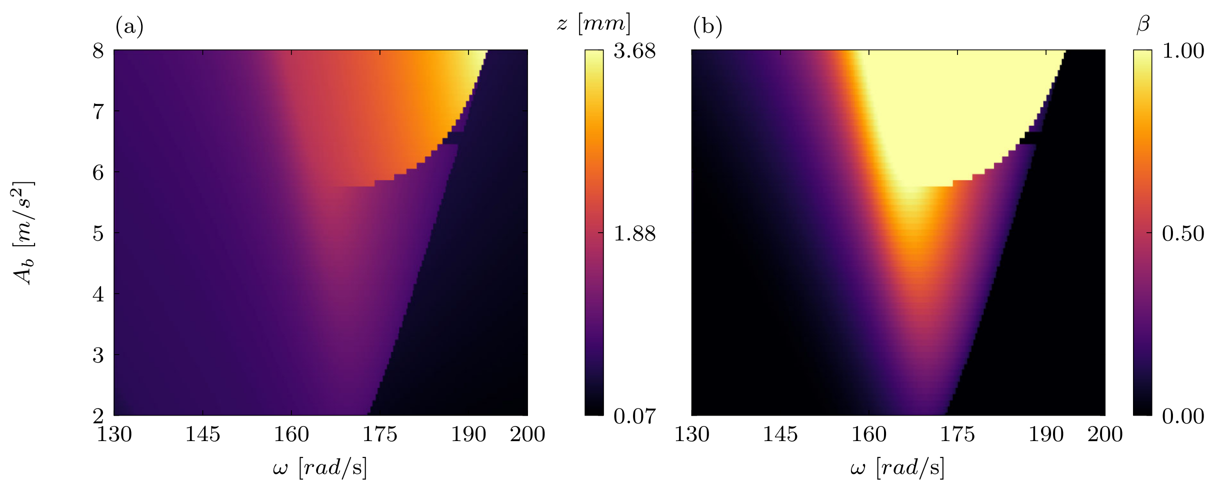

Fig. 11 Maximum distribution surface in therms of frequency ω and base acceleration amplitude A_b. **a** Relative displacement. **b** Martensite volume fraction

Figure 12a also highlights a region for $A_b = 6\,\text{m/s}^2$ around 107 to 126 rad/s where the system shifts from a period-1 to a period-2 orbit. Note that the harvester maximum output power response is even higher than for $A_b = 8\,\text{m/s}^2$. Figure 12e shows the relative displacement for $\omega = 110$ rad/s while Fig. 12 f and g present the output power and phase space with the Poincaré sections, respectively. Figure 13c and d show incomplete phase transformation through stress–strain curve and martensite volume fraction times series. The phase transformation can contribute to increase the nonlinear response which can be associated with the changes in the stopper mechanical properties promoted when contact occurs.

Figure 14a evaluates the harvester output power frequency response when base amplitude is $A_b = 6$ m/s^2 and another regions are highlighted for analysis. It takes an interval from 178 to 188 to evaluate a region where the harvester performance can abruptly changes presenting dynamical jumps and phase transformations.

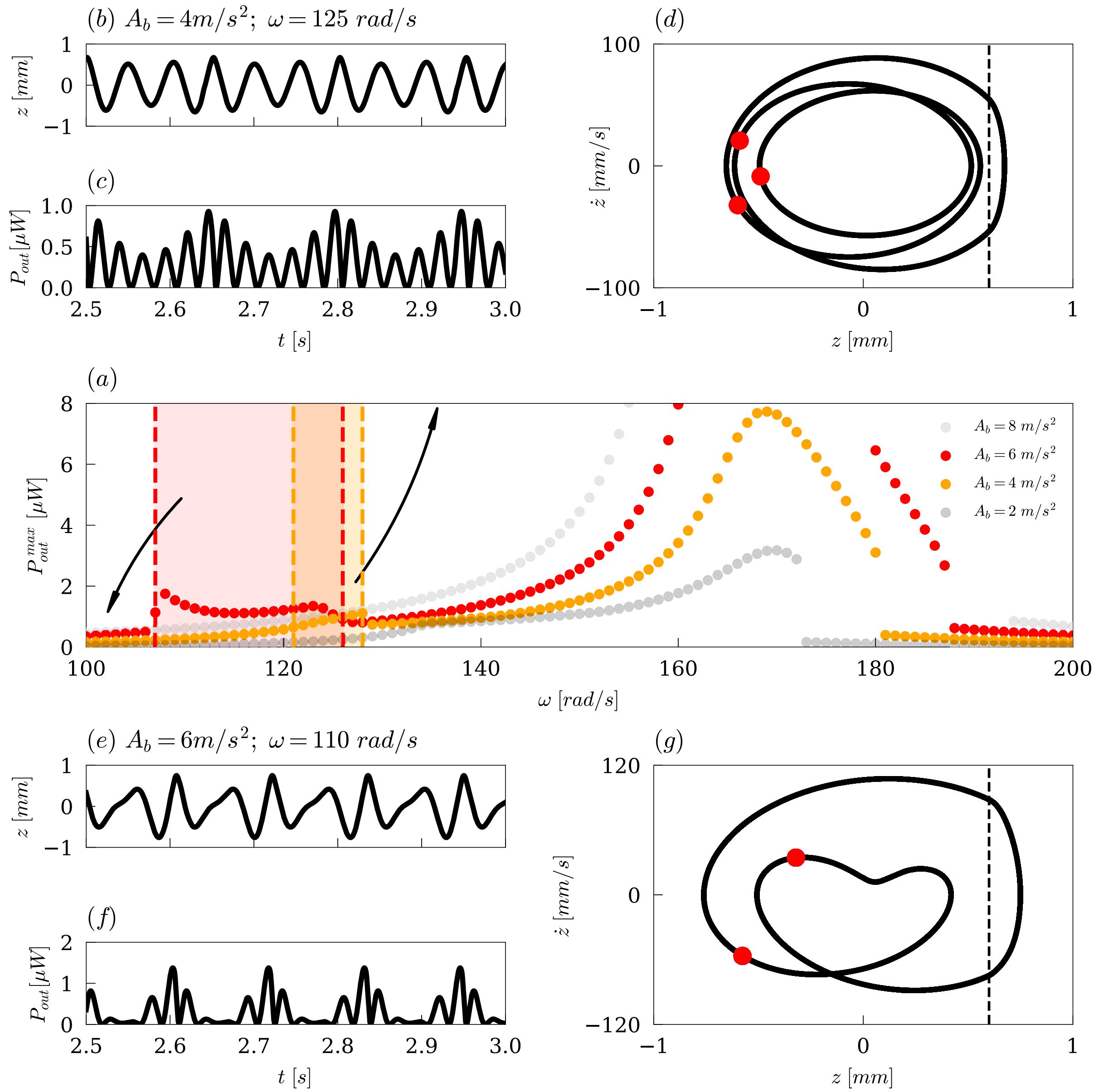

Fig. 12 Harvester dynamical response for constant SMA stopper temperature and fixed gap distance. **a** Maximum output power frequency response for different values of base acceleration amplitudes. **b** Relative displacement in steady state response for stationary $\omega = 125$ rad/s and $A_b = 4\,\mathrm{m/s^2}$. **c** Output power. **d** Phase space. **e** Relative displacement in steady state response for stationary $\omega = 110$ rad/s and $A_b = 6\,\mathrm{m/s^2}$. **f** Output power. **g** Phase space

Figure 14b, c and d illustrate this behavior for $\omega = 178$ rad/s, presenting the higher orbit amplitude and complete phase transformation due to contact, $\omega = 183$ rad/s presenting incomplete phase transformation. Finally, for $\omega = 188$ rad/s, no contact occurs leading the system to a small orbit response. Figure 13e presents the stress–strain diagram when the contact occurs for this three last condition of forcing frequency while Fig. 13f is associated with the martensitic volume fraction time series. Note that for $\omega = 188$ rad/s, no phase transformation occurs since contact does not occurs neither.

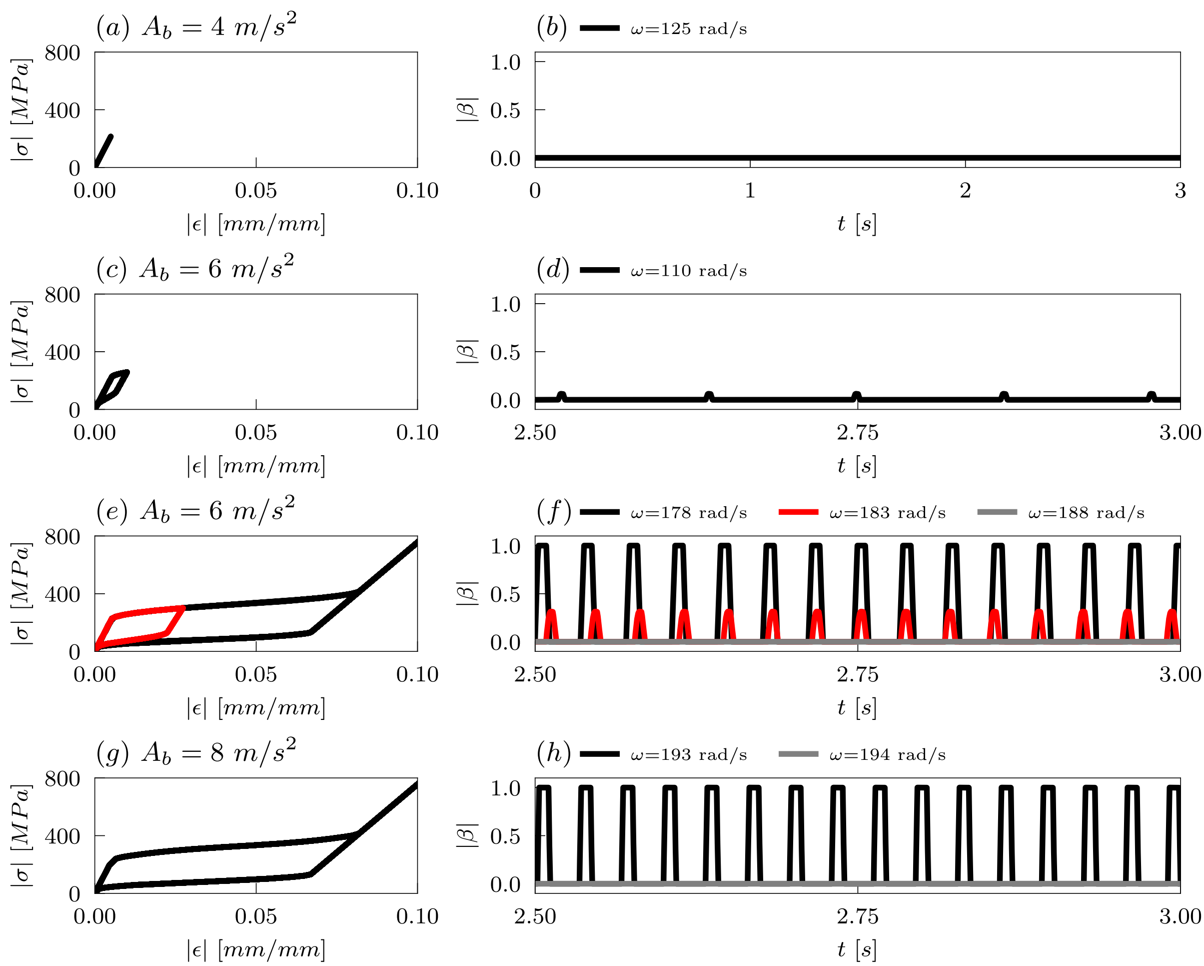

Fig. 13 SMA stopper response in highlighted steady state forcing frequencies ω and base amplitudes A_b. **a**, **c**, **e** and **g** stress $\sigma \times$ strain ϵ diagrams. **b**, **d**, **f** and **h** martensite volume fraction β

The maximum output power occurs at $\omega = 179$ rad/s associated with 30 µW.

A condition for $A_b = 8\,\text{m/s}^2$ is now of concern (Fig. 15a). The frequency response presents two visible slopes where the first one is between 140 to 160 rad/s, being associated with contacts with incomplete phase transformations. The second slope remains from 161 to 193 rad/s, where a complete martensitic phase is achieved during the contact. The maximum output power of 100 µW is found at $\omega = 193$ rad/s followed by a dynamical jump when the harvester performance drops to small values. Figure 15a–c evaluate the system performance in a interval of 1 rad/s enhancing the considerable changes in dynamical response. Note that, in Fig. 15b and d, the relative displacement total amplitude goes from 3.68 mm to −6.54 mm in a total of 10.22 mm for $A_b = 8\,\text{m/s}^2$.

3.3 Comparative analysis

As an overall comparative analysis, three different configurations are investigated: a linear harvester, where contact does not occur; a nonsmooth harvester, with constant gap distance and stiffness related to E_A; and an adaptive harvester, with a gap that can vary. The investigation evaluates the harvester performance through SMA phase transformations induced by temperature and mechanical loads.

Figure 16a compares the shifts in frequency ω with respect to the base amplitude, showing the maximum

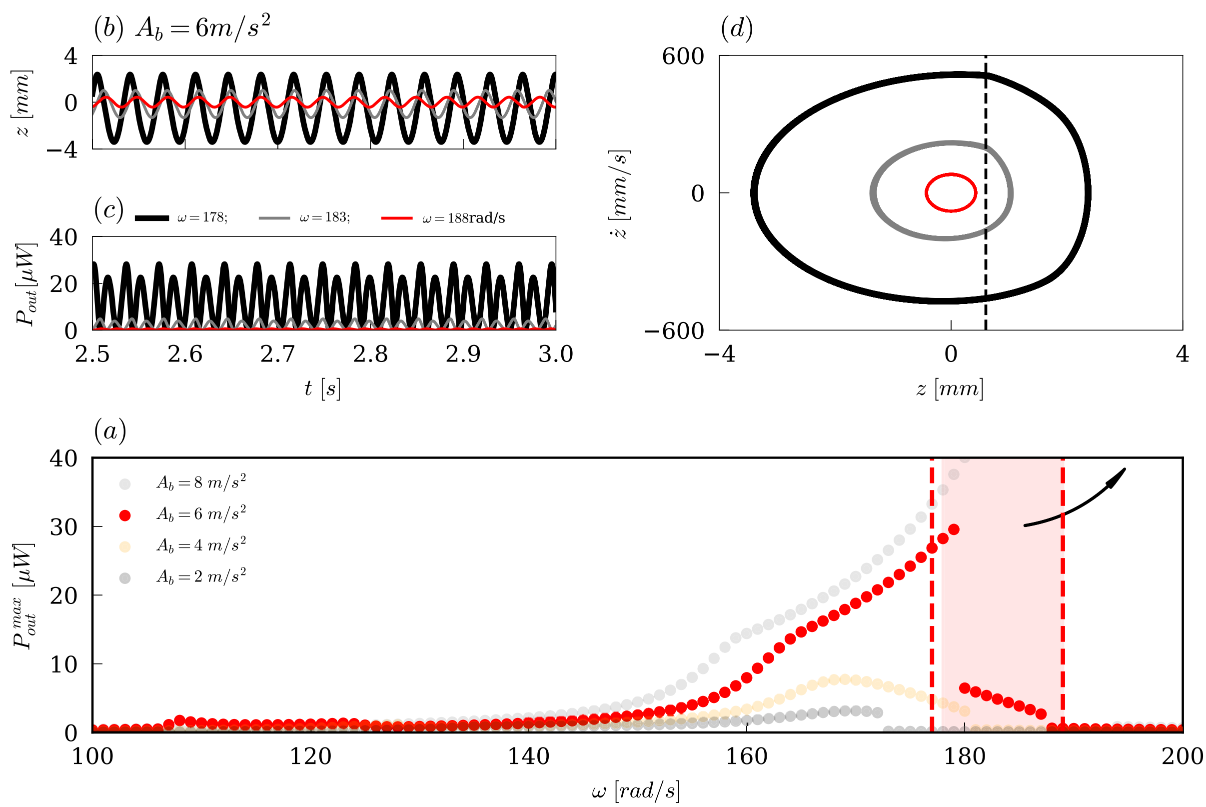

Fig. 14 Harvester dynamical response for constant SMA stopper temperature and fixed gap distance. **a** Maximum output power frequency response for different values of base acceleration amplitudes. **b** Relative displacement in steady state response for stationary $\omega = 178$, 183 and 188 rad/s and $A_b = 6\,\text{m/s}^2$. **c** Output power. **d** Phase space

peak of output power. The linear harvester does not present change with respect to its maximum peak. By considering the harvester with constant gap stopper, the frequency peak tends to increase from 186 rad/s due to the hardening effect promoted by the contact where both stiffness from the beam and the support act together. These value tends to reach a plateau around 224 rad/s when the base amplitude becomes significant and the contact occurs for basically all frequencies in the evaluated range. The harvester with adaptive SMA stopper presents the possibility to shift its ω peak due to the shape memory effect in a region until $A_b = 1\,\text{m/s}^2$ where the gap distance varies and the peak frequency shifts from 146 to 186 rad/s according to the SMA temperature.

After that, until $A_b = 8\,\text{m/s}^2$, nonlinear effects become more evident since phase transformations are responsible for a softening effect. It is important to note that the start and finish of SMA critical stress can also be adjusted by the temperature, allowing one to move from the black dots to the blue dots by increasing even more the SMA temperature to $T >> A_f$. At this point, the critical stresses become high in such a way that phase transformation cannot occur anymore and the adaptive harvester achieves the same condition of the one with constant gap. Afterward, the stopper with constant gap presents a shift with respect to the frequency of 38 rad/s (from 186 to 224) while the adaptive stopper presents a shift of 78 rad/s (from 146 to 224).

Figure 16b presents the maximum martensitic volume fraction formed for each base amplitude. This result is interesting to determine the regions where complete or incomplete phase transformations occur. Figure 16c presents the maximum relative displacement of the stopper indicating how the stopper can limit the maximum amplitude of the harvester operation. The nonsmooth harvester with constant gap and the one with adaptive stopper present low maximum ampli-

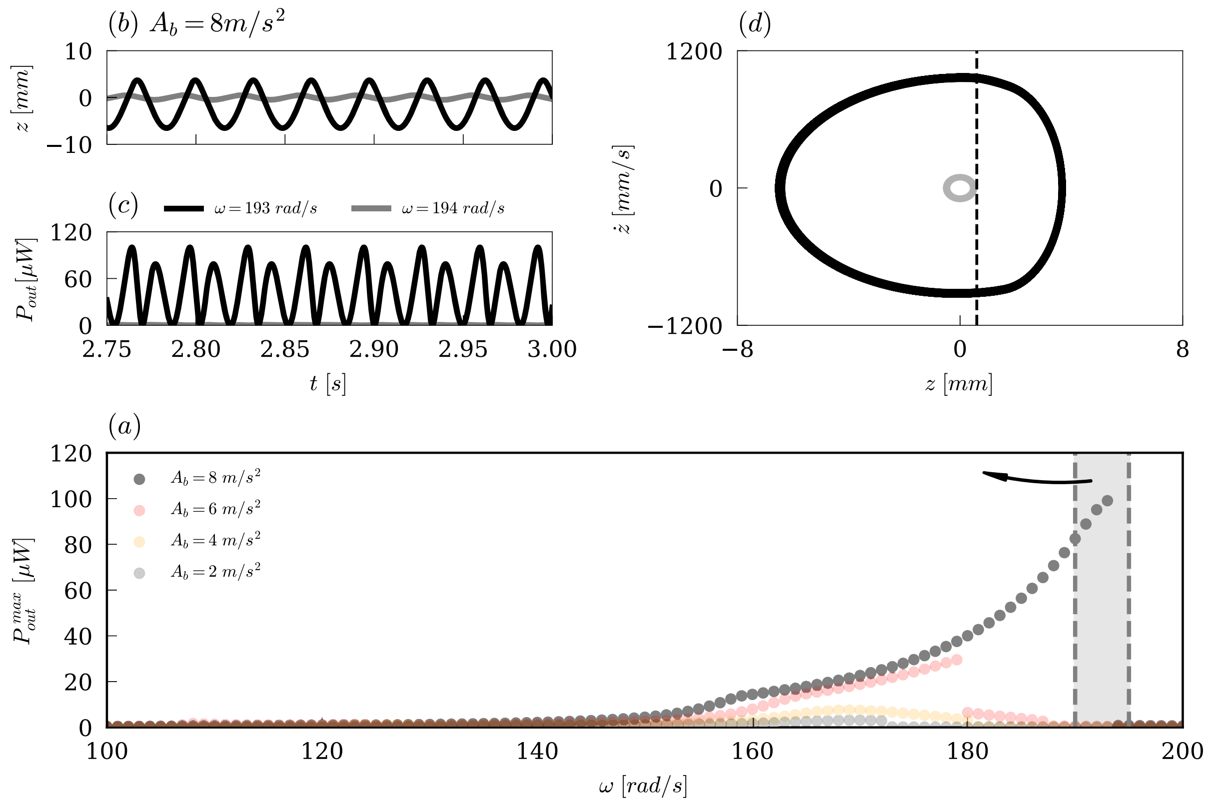

Fig. 15 Harvester dynamical response for constant SMA stopper temperature and fixed gap distance. **a** Maximum output power frequency response for different values of base acceleration amplitudes. **b** Relative displacement in steady state response for stationary $\omega = 193$, and 194 rad/s and $A_b = 8$ m/s^2. **c** Output power. **d** Phase space

tudes when compared with the linear harvester. Two phenomena explains this behavior: the hysteretic dissipation that attenuates the maximum amplitude; and the softening effect attributed to pseudoelasticity which tends to increase the amplitude. Comparing the system with elastic stopper with the one with adaptive stopper for similar amplitudes and strains, the martensitic phase transformations require less force to achieve the same condition, which ensures safety and reliability.

Figure 16d shows the maximum output power for each specific value of base vibration amplitude. It is noticeable that stress-induced phase transformations and energy dissipation have a great influence on system performance. Once again, by increasing the SMA temperature to values $T >> A_f$, it is possible to avoid stress-induced phase transformation and move from the black curve to the blue curve. This result can lead to an output power close to a linear harvester with the possibility to adapt according to external changes.

4 Conclusions

This paper proposes a novel adaptive nonsmooth energy harvester that synergistically combines piezoelectric and SMA elements. The SMA morphing ability is exploited to change the gap distance, altering the system nonlinearity. The harvester is modeled as a nonsmooth oscillator, with an SMA stopper, connected to an electrical circuit by a piezoelectric element. The SMA thermomechanical behavior is described by a constitutive model with assumed polynomial phase transformation kinetics. Numerical simulations are carried out considering the SMA nonsmooth system exploiting two situations: the gap adaptiveness induced by the two-way shape memory effect; pseudoelastic hysteretic dissipation due to stress-induced phase transformation. A parametric investigation is developed varying forcing frequency and amplitude, suggesting specific conditions where the SMA phase transformation is capable

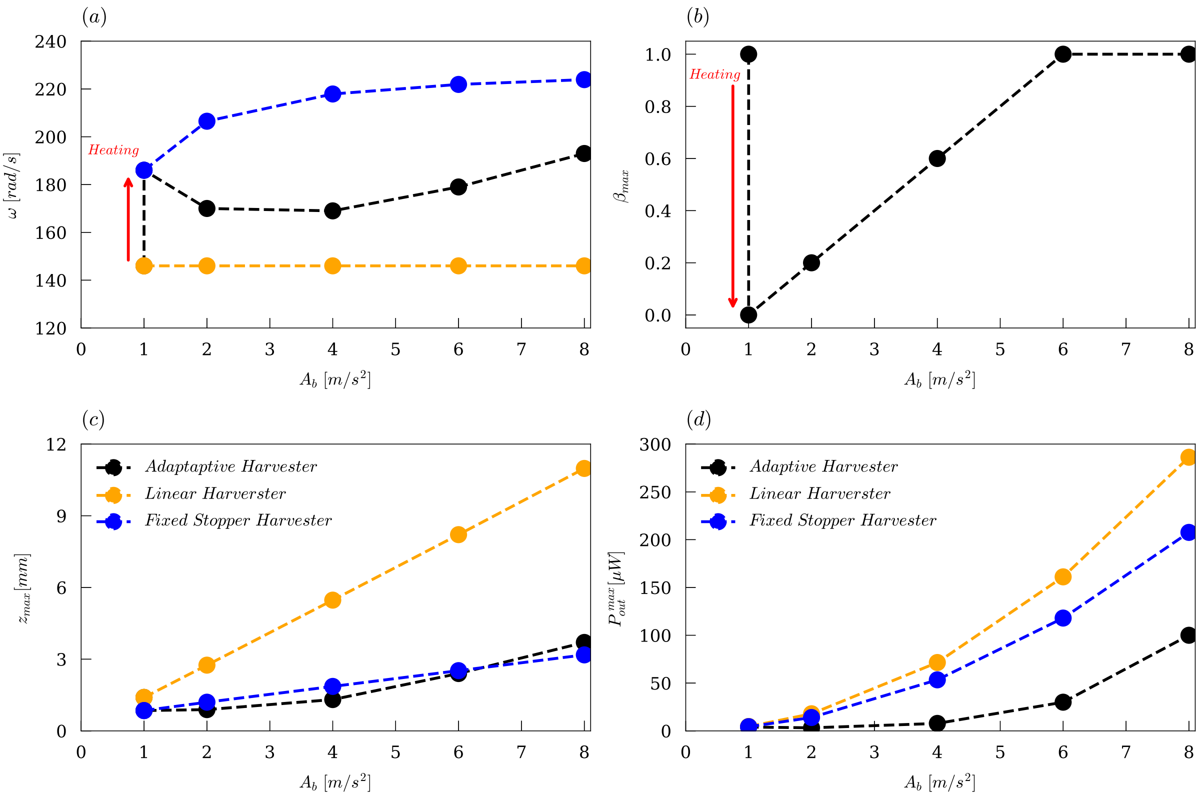

Fig. 16 Comparative analysis concerning different designs of piezoelectric nonsmooth energy harvesters by capturing the maximum peaks for evaluated base acceleration amplitudes A_b conditions. **a** Frequency ω of peaks. **b** Martensite volume fraction. **c** Maximum displacement. **d** Output power obtained in peaks

to improve the energy harvesting capacity due to nonsmoothness.

The gap control allows interactions between the harvester capacity and ambient changes. A broader frequency bandwidth is observed due to nonsmooth behavior. But there is a competition between broadband and amplitude that needs to be carefully adjusted based on the dynamical perspective. Results show that a change on ambient sources can be overcome by proper gap distances, induced by SMA.

In a different perspective, stress-induced phase transformations are evaluated by considering hysteretic energy dissipation due to pseudoelastic effect. This situation can significantly contribute to the increase of the maximum output power and also limits critical responses. SMA pseudoelastic behavior promotes complex responses, represented by dynamical jumps.

A comparative analysis considering three configurations is developed: a linear harvester, where contact does not occur; a nonsmooth harvester, with constant gap distance and stiffness; and an adaptive harvester, with gap that changes. Results show that the nonlinear harvesters present a broadband over the linear harvester performing in different conditions of forcing frequency and base amplitudes. On this basis, the SMA adaptive harvester presents the ability to shift its operational range according to temperature and can also prevent failure due to hysteresis.

In summary, the adaptive energy harvester with SMA stopper is an innovative and promising idea for further developments of energy harvesting devices. Nevertheless, the nonlinearities involved are responsible for complex dynamical behavior and therefore, a in-depth understanding of nonlinear dynamics is essential for the system design. Besides, it is important to investigate the fatigue life related to the device since contacts can dramatically alter its lifespan.

Funding The authors would like to acknowledge the support of the Brazilian Research Agencies CNPq (Conselho Nacional de Desenvolvimento Científico e Tecnológico), CAPES (Coordenação de Aperfeiçoamento de Pessoal de Nível Superior) and FAPERJ (Fundação Carlos Chagas Filho de Amparo à Pesquisa do Estado do Rio de Janeiro) and through the INCT-EIE (National Institute of Science and Technology - Smart Structures in Engineering), CNPq, CAPES and FAPEMIG (Fundação de Amparo à Pesquisa do Estado de Minas Gerais). The support of the AFOSR (Air Force Office of Scientific Research) (FA9550-23-1-0527) is also acknowledged.

Data Availability Statement The datasets generated during and/or analyzed during the current study are available from the corresponding author upon reasonable request.

Declarations

Conflict of interest The authors declare that they have no conflict of interest.

References

1. Adeodato, A., Duarte, B.T., Monteiro, L.L.S., Pacheco, P.M.C.L., Savi, M.A.: Synergistic use of piezoelectric and shape memory alloy elements for vibration-based energy harvesting. Int. J. Mech. Sci. **194**, 106206 (2021). https://doi.org/10.1016/j.ijmecsci.2020.106206
2. Adeodato, A., Vignoli, L.L., Paiva, A., Monteiro, L.L.S., Pacheco, P.M.C.L., Savi, M.A.: A shape memory alloy constitutive model with polynomial phase transformation kinetics. Shape Memory and Superelasticity (2022). https://doi.org/10.1007/s40830-022-00382-1
3. Adeodato A., Abhijeet, M.G., Piotr, W., Grzegorz, L.: Dynamics of a piezoelectric vibration energy harvester with a pseudoelastic SMA spring. AIP Adv. (2024). https://doi.org/10.1063/5.0194519
4. Ai, R., Monteiro, L.L.S., Monteiro, P.C.C., Jr., Pacheco, P.M.C.L., Savi, M.A.: Piezoelectric vibration-based energy harvesting enhancement exploiting nonsmoothness. Actuators **1**, 25 (2019). https://doi.org/10.3390/act8010025
5. Almeida, S.F., Vignoli, L.L.: Influence of operating conditions in nonlinear vibration of a drill-string. Proceed. Institut. Mech. Eng., Part M: J. Eng. Marit. Environ. **239**(1), 133–144 (2025). https://doi.org/10.1177/14750902241254144
6. Anton, S.R., Sodano, H.A.: A review of power harvesting using piezoelectric materials (2003–2006). Smart Mater. Struct. **16**, R1 (2007). https://doi.org/10.1088/0964-1726/16/3/R01
7. Ben Zohra, M., Riad, A., Azelmad, E., Alhamany, A.: Improving energy harvesting by integrating smart materials into road infrastructure. J. Eng. Res. (2025). https://doi.org/10.1016/j.jer.2025.01.003
8. Blystad, L.C.J., Halvorsen, E.: A piezoelectric energy harvester with a mechanical end stop on one side. Microsyst. Technol. **17**(4), 505–511 (2011). https://doi.org/10.1007/s00542-010-1163-0
9. Brinson, L.C.: One-dimensional constitutive behavior of shape memory alloys: Thermomechanical derivation with non-constant material functions and redefined martensite internal variable. J. Intell. Mater. Syst. Struct. **4**(2), 229–242 (1993). https://doi.org/10.1177/1045389X9300400213
10. Caetano, V. J., Savi, M. A.: Star-shaped piezoelectric mechanical energy harvesters for multidirectional sources. International Journal of Mechanical Sciences, 215: 106962, 2022. ISSN 0020-7403. https://doi.org/10.1016/j.ijmecsci.2021.106962. https://www.sciencedirect.com/science/article/pii/S002074032100672X
11. Cao, Q., Wiercigroch, M., Pavlovskaia, E., Thompson, J.M.T., Grebogi, C.: Piecewise linear approach to an archetypal oscillator for smooth and discontinuous dynamics. Philosoph. Trans. Royal Soci. A: Math., Phys. Eng. Sci. **366**(1865), 635–652 (2007). https://doi.org/10.1098/rsta.2007.2115
12. Chen, K., Gao, Q., Fang, S., Zou, D., Yang, Z., Liao, W.H.: An auxetic nonlinear piezoelectric energy harvester for enhancing efficiency and bandwidth. Appl. Energy **298**, 117274 (2021). https://doi.org/10.1016/j.apenergy.2021.117274
13. Chen, W., Lu, J., Tan, X., Albertelli, P., He, H.: Comprehensive analysis of a butterfly-shaped piezoelectric shunting vibration absorber for robust vibration reduction and isolation: Theoretical and experimental validation. Mech. Syst. Signal Process. **223**, 111843 (2025). https://doi.org/10.1016/j.ymssp.2024.111843
14. Costa, L.G., Savi, M.A.: Nonlinear dynamics of a compact and multistable mechanical energy harvester. Int. J. Mech. Sci. **262**, 108731 (2024). https://doi.org/10.1016/j.ijmecsci.2023.108731
15. De Sousa, V.C., de Marqui, C.J.: Airfoil-based piezoelectric energy harvesting by exploiting the pseudoelastic hysteresis of shape memory alloy springs. Smart Mater. Struct. **24**(12), 125014 (2015). https://doi.org/10.1088/0964-1726/24/12/125014
16. Din, I.U., Medhin, Y., Aslam, N., Bathusha, M.S.S., Umer, R., Khan, K.A.: Rate dependent piezoresistive characterization of smart aerospace sandwich structures embedded with reduced graphene oxide (rgo) coated fabric sensors. Composit. Commun. **36**, 101382 (2022). https://doi.org/10.1016/j.coco.2022.101382
17. Divenyi, S., Savi, M.A., Weber, H.I., França, L.F.P.: Experimental investigation of an oscillator with discontinuous support considering different system aspects. Chaos, Solit. Fractals **38**(3), 685–695 (2008). https://doi.org/10.1016/j.chaos.2007.01.005
18. Divenyi, S., Savi, M.A., Wiercigroch, M., Pavlovskaia, E.: Drill-string vibration analysis using non-smooth dynamics approach. Nonlinear Dyn. **70**, 1017–1035 (2012). https://doi.org/10.1007/s11071-012-0510-3
19. dos Santos, B.C., Savi, M.A.: Nonlinear dynamics of a nonsmooth shape memory alloy oscillator. Chaos, Solitons Fractals **40**, 197–209 (2019). https://doi.org/10.1016/j.chaos.2007.07.058
20. Enyan, M., Bing, Z., Amu-Darko, J.N.O., Issaka, E., Otoo, S.L., Agyemang, M.F.: Advances in smart materials soft actuators on mechanisms, fabrication, materials, and multifaceted applications: A review. J. Thermopl. Compos. Mater. **38**(1), 302–370 (2025). https://doi.org/10.1177/08927057241248028
21. Erturk, A., Inman, D.J.: On mechanical modeling of cantilevered piezoelectric vibration energy harvesters. Journal of Intelligent Material Systems and Structures (2008). https://doi.org/10.1177/1045389X07085639

22. Gawron, P., Wendt, T.M., Rupitsch, S.J.: Additively manufactured multi-material cantilever for electromagnetic vibration harvesting. IEEE Sensors Journal (2025). https://doi.org/10.1109/JSEN.2025.3526541
23. Halim, M.A., Park, J.Y.: Theoretical modeling and analysis of mechanical impact driven and frequency up-converted piezoelectric energy harvester for low-frequency and wide-bandwidth operation. Sens. Actuators, A **208**, 56–65 (2014). https://doi.org/10.1016/j.sna.2013.12.033
24. Hu, G., Tang, L., Das, R., Marzocca, P.: A two-degree-of-freedom piezoelectric energy harvester with stoppers for achieving enhanced performance. Int. J. Mech. Sci. **149**, 500–507 (2018). https://doi.org/10.1016/j.ijmecsci.2017.07.051
25. Karpenko, E.V., Wiercigroch, M., Pavlovskaia, E., Cartmell, M.P.: Piecewise approximate analytical solutions for a jeffcott rotor with a snubber ring. Int. J. Mech. Sci. **44**(3), 475–488 (2002). https://doi.org/10.1016/S0020-7403(01)00108-4
26. Kim, P., Seok, J.: A multi-stable energy harvester: dynamic modeling and bifurcation analysis. J. Sound Vibrat. **333**(21), 5525–5547 (2014). https://doi.org/10.1016/j.jsv.2014.05.054
27. Lagoudas, D.: Shape Memory Alloys. Springer, USA (2008)
28. Li, H.T., Qin, W.Y., Zu, J., Yang, Z.: Modeling and experimental validation of a buckled compressive-mode piezoelectric energy harvester. Nonlinear Dyn. **92**, 1761–1780 (2018). https://doi.org/10.1007/s11071-018-4160-y
29. Liu, H., Lee, C., Kobayashi, T., Tai, C.J., Quan, C.: Investigation of a mems piezoelectric energy harvester system with a frequency-widened-bandwidth mechanism introduced by mechanical stoppers. Smart Mater. Struct **21**, 035005 (2012a). https://doi.org/10.1088/0964-1726/21/3/035005
30. Liu, H., Lee, C., Kobayashi, T., Tai, C.J., Quan, C.: Piezoelectric mems-based wideband energy harvesting systems using a frequency-up-conversion cantilever stopper. Sens. Actuat. A Phys. **186**, 242–248 (2012). https://doi.org/10.1016/j.sna.2012.01.033
31. Liu, S., Cheng, Q., Zhao, D., Feng, L.: Theoretical modeling and analysis of two-degree-of-freedom piezoelectric energy harvester with stopper. Sens. Actuat. A **245**, 97–105 (2016). https://doi.org/10.1016/j.sna.2016.04.060
32. Liu, Y., Wiercigroch, M., Pavlovskaia, E., Yu, H.: Modelling of a vibro-impact capsule system. Int. J. Mech. Sci. **66**, 2–11 (2013). https://doi.org/10.1016/j.ijmecsci.2012.09.012
33. Liu, Y., Pavlovskaia, E., Wiercigroch, M., Peng, Z.: Forward and backward motion control of a vibro-impact capsule system. Int. J. Non-Linear Mech. **70**, 30–46 (2015). https://doi.org/10.1016/j.ijnonlinmec.2014.10.009
34. Liu, Y., Pavlovskaia, E., Wiercigroch, M.: Experimental verification of the vibro-impact capsule model. Nonlinear Dyn. **83**, 1029–1041 (2016). https://doi.org/10.1007/s11071-015-2385-6
35. Ma, Y., Ing, J., Banerjee, S., Wiercigroch, M., Pavlovskaia, E.: The nature of the normal form map for soft impacting systems. Int. J. Non-Linear Mech. **43**(6), 504–513 (2008). https://doi.org/10.1016/j.ijnonlinmec.2008.04.001
36. Muscat, A., Bhattacharya, S., Zhu, Y.: Electromagnetic vibrational energy harvesters: a review. Sensors (2022). https://doi.org/10.3390/s22155555
37. Naderi, A., Fakher, M., Hosseini-Hashemi, S.: On the local/nonlocal piezoelectric nanobeams: Vibration, buckling, and energy harvesting. Mech. Syst Signal Process. **151**, 107432 (2021). https://doi.org/10.1016/j.ymssp.2020.107432
38. Oudich, A., Thiebaud, F.: A two-way shape memory alloy-piezoelectric bimorph for thermal energy harvesting. Mech. Mater. **102**, 1–6 (2016). https://doi.org/10.1016/j.mechmat.2016.08.006
39. Paez, C.J., Pavlovskaia, E., Wiercigroch, M.: Bifurcation analysis of a piecewise-linear impact oscillator with drift. Nonlinear Dyn. **77**, 213–227 (2014). https://doi.org/10.1007/s11071-014-1285-5
40. Paiva, A., Savi, M.A.: A constitutive model for shape memory alloys considering tensile-compressive asymmetry and plasticity. Int. J. Solids Struct. **42**(11–12), 3439–3457 (2005). https://doi.org/10.1016/j.ijsolstr.2004.11.006
41. Pavlovskaia, E., Wiercigroch, M., Woo, K.C., Rodger, A.A.: Modelling of ground moling dynamics by an impact oscillator with a frictional slider. Meccanica **38**, 85–97 (2003). https://doi.org/10.1023/A:1022023502199
42. Pavlovskaia, E., Ing, J., Wiercigroch, M., Banerjee, S.: Complex dynamics of bilinear oscillator close to grazing. Int. J. Bifurcat. Chaos **20**(11), 3801–3817 (2010). https://doi.org/10.1142/S0218127410028069
43. Pavlovskaia, E., Hendry, D.C., Wiercigroch, M.: Modelling of high frequency vibro-impact drilling. Int. J. Mech. Sci. **91**, 110–119 (2015). https://doi.org/10.1016/j.ijmecsci.2013.08.009
44. Prajwal, K.T., Manickavasagam, K., Suresh, R.: A review on vibration energy harvesting technologies: analysis and technologies. Eur. Phys. J. Special Topics **231**(8), 1359–1371 (2022). https://doi.org/10.1140/epjs/s11734-022-00490-0
45. Safaei, K., Abedi, H., Nematollahi, M., Kordizadeh, F., Dabbaghi, H., Bayati, P., Javanbakht, R., Jahadakbar, A., Elahinia, M., Poorganji, B.: Additive manufacturing of niti shape memory alloy for biomedical applications: review of the LPBF process ecosystem. JOM (2021). https://doi.org/10.1007/s11837-021-04937-y
46. Savi, M.A.: Nonlinear dynamics and chaos in shape memory alloy systems. Int. J. Non-Linear Mech. (2015). https://doi.org/10.1016/j.ijnonlinmec.2014.06.001
47. Savi, M.A., Divenyi, S., França, L.F.P., Weber, H.I.: Numerical and experimental investigations of the nonlinear dynamics and chaos in non-smooth systems. J. Sound Vib. **301**(1–2), 59–73 (2007). https://doi.org/10.1016/j.jsv.2006.09.014
48. Senthilkumar, M., Vasundhara, M.G., Kalavathi, G.K.: Electromechanical analytical model of shape memory alloy based tunable cantilevered piezoelectric energy harvester. Int. J. Mech. Mater. Des. **15**(3), 611–627 (2019). https://doi.org/10.1007/s10999-018-9413-x
49. Shahsavar, M., Ashory, M.R., Khatibi, M.M.: Increasing the efficiency of a bistable cantilever beam energy harvester exploiting vibro-impact effects. J. Intell. Mater. Syst. Struct. **34**(6), 717–732 (2023). https://doi.org/10.1177/1045389X221115703
50. Silva, L.C., Savi, M.A., Paiva, A.: Nonlinear dynamics of a rotordynamic nonsmooth shape memory alloy system. J. Sound Vib. **332**, 608–621 (2013)
51. Silva, L.L., Oliveira, S.A., Pacheco, P.M.C.L., Savi, M.A.: Synergistic use of smart materials for vibration-based energy

harvesting. Eur. Phys. J. Special Topics **224**, 3005–3021 (2015). https://doi.org/10.1140/epjst/e2015-02603-8
52. Su, M., Xu, W., Zhang, Y.: Theoretical analysis of piezoelectric energy harvesting system with impact under random excitation. Int. J. Non-Linear Mech. **119**, 103322 (2020). https://doi.org/10.1016/j.ijnonlinmec.2019.103322
53. Sun, S., Leng, Y., Hur, S., Sun, F., Chen, X., Song, H.-C., Kang, C.-Y.: Force and stability mechanism analysis of two types of nonlinear mono-stable and multi-stable piezoelectric energy harvesters using cantilever structure and magnetic interaction. Smart Mater. Struct. **32**(3), 035003 (2023). https://doi.org/10.1088/1361-665X/acb1e3
54. Thomas, K.K., Hassan, N.M., Bahroun, Z., Awad, M.: Exploring the role of shape memory alloys in advanced composite sandwich panels and laminates. Composit. Part C Open Access **16**, 100557 (2025). https://doi.org/10.1016/j.jcomc.2025.100557
55. du Toit, N.E.: Modeling and design of a MEMS piezoelectric vibration energy harvester. Phd, Massachusetts Institute of Technology, United States of America (2005)
56. Tran, N., Ghayesh, M.H., Arjomandi, M.: Ambient vibration energy harvesters: A review on nonlinear techniques for performance enhancement. Int. J. Eng. Sci. **127**, 162–185 (2018). https://doi.org/10.1016/j.ijengsci.2018.02.003
57. Triplett, A., Quinn, D.D.: The effect of non-linear piezoelectric coupling on vibration-based energy harvesting. J. Intell. Mater. Syst. Struct. **20**(16), 1959–1967 (2009). https://doi.org/10.1177/1045389X09343218
58. Viet, N.V., Zaki, W., Umer, R.: Analytical investigation of an energy harvesting shape memory alloy-piezoelectric beam. Arch. Appl. Mech. **90**, 2715–2738 (2020). https://doi.org/10.1007/s00419-020-01745-9
59. Wang, J., Chang, Z., Liu, T., Chen, L.: A review of linear and nonlinear vibration analysis of composite laminated structures by computational approaches: 2015–2024. Nonlinear Dyn. (2025). https://doi.org/10.1007/s11071-024-10837-y
60. Wang, Y., Yang, Z., Cao, D.: Distributed-parameter modeling and dynamic analysis of rotational compressive-mode energy harvesters. Nonlinear Dyn. **103**(1), 157–182 (2021). https://doi.org/10.1007/s11071-020-06144-x
61. Williams, C.B., Yates, R.B.: Analysis of a micro-electric generator for microsystems. Sens. Actuat., a Phys. **52**, 8–11 (1996). https://doi.org/10.1016/0924-4247(96)80118-X
62. Yang, Z., Zhou, S., Zu, J., Inman, D.: High-performance piezoelectric energy harvesters and their applications. Joule **2**(4), 642–697 (2018). https://doi.org/10.1016/j.joule.2018.03.011
63. Yotov, I., Todorov, G., Gieva, E., Todorov, T.: Dynamics of a self-excited vibrating thermal energy harvester with shape memory alloys and PVDF cantilevers. Actuators, 14 (1), 2025. ISSN 2076-0825. https://www.mdpi.com/2076-0825/14/1/8
64. Zareie, S., Alam, M.S., Seethaler, R.J., Zabihollah, A.: Effect of shape memory alloy-magnetorheological fluid-based structural control system on the marine structure using nonlinear time-history analysis. Appl. Ocean Res. **91**, 101836 (2019). https://doi.org/10.1016/j.apor.2019.05.021
65. Zhou, K., Dai, H.L., Abdelkefi, A., Ni, Q.: Theoretical modeling and nonlinear analysis of piezoelectric energy harvesters with different stoppers. Int. J. Mech. Sci. **166**, 105233 (2020). https://doi.org/10.1016/j.ijmecsci.2019.105233
66. Zhou, S., Lallart, M., Erturk, A.: Multistable vibration energy harvesters: principle, progress, and perspectives. J. Sound Vibrat. **528**, 116886 (2022). https://doi.org/10.1016/j.jsv.2022.116886